Modeling Measurements of Black Body Radiation to Understand Data Provided by ALMA Satellites

WPI

A Major Qualifying Project Submitted to the
Faculty of Worcester Polytechnic Institute
in partial fulfillment of the requirements
for the Degree in Bachelor of Science In Physics

By:
Nickolas Gardner
Nicole Garay

Project Advisor:
Professor Douglas Petkie, WPI

Abstract

This research project aimed to become familiar with how blackbody radiation is studied in space. We sought to model a more small-scale experiment with similar instruments to the ALMA telescope, a facility used to explore different parts of the universe. Our experiment included a heterodyne receiver, amplifier, detector, optical chopper, an analog lock-in and a blackbody source. In this way, our team gained hands-on experience by collecting data to relate changes in temperature related to detecting blackbody radiation. In understanding part of the internal workings of the ALMA satellite, we can better understand how blackbody radiation from supergiant stars is studied and used to predict information from thermal sources that are lightyears away, such as the temperature of stars, what chemicals make up a star, and the lifespan of a star.

Acknowledgments

First and foremost, we would like to thank Dr. Doug Petkie for being a fantastic advisor in this process. Doug came to our aid when we decided we wanted to have a more hands-on experience rather than sticking to the traditional theoretical side of astrophysics. He inspired the design for the experiment and helped us even more by ordering the parts necessary to make the system function. His guidance helped us develop a successful proof of concept for an experiment that can be expanded on by future students working in the lab. Dr. Petkie also provided valuable tools for graphical analysis and helped us through the complicated equations necessary for conducting the experiment.

We would also like to thank Jacob Bouchard for being a role model in the lab. His quick thinking and experience with LabVIEW and the machines we were working with allowed him to bring us up to speed on how experiments in the lab are to be conducted. Jacob made going to the lab enjoyable even after our long experiments were unsuccessful at times. With his help we were finally able to come up with a working experiment and gained the hands-on experience we were looking for.

Table of Content

List of Figures

1. Introduction

In the past decade, astronomers have made great strides to further the understanding of our observable universe. Most of the research related to this was possible through sophisticated technological advancements and dedicated professionals. Astronomical projects like the Atacama Millimeter/submillimeter Large Array (ALMA) use specialized radio telescopes worth 1,400 million dollars. To best understand how these telescopes are a vital factor in our knowledge about the universe, we need to develop a hands-on model that we can interact with at an appropriate time frame.

This initiative required a greater familiarity with mathematical principles relating to light properties, blackbody thermal radiation laws, and molecular energy. In addition, a technical understanding of the structure of ALMA telescopes to gather and analyze signals from space. Our research allowed us to create an educational model of ALMA's technologies that examine blackbody radiation sources such as supergiant stars and black holes. Using a simulated blackbody source, we performed trials to comprehend the relationship between the temperature of a body and the energy it produces. Executing these trials allowed us to construct a working model that provided the insight we needed about ALMA.

It's clear that the field of astronomy is growing exponentially to untangle the mysteries regarding the evolutions of our universe. ALMA's efforts involve studying blackbody sources that essentially help recycle and produce celestial objects. Learning about this allowed us to assemble a model that shows the correlation of a blackbody's temperature change to its voltage change. This knowledge is essential since it provides understanding regarding the life cycle of supergiant stars and their role in galaxy evolution. With more knowledge available than ever before, astronomers play a necessary part in our perception of the universe.

2. Background

This chapter aims to briefly explain the electromagnetic spectrum in a physical and chemical sense. Then we explain how it's currently used for submillimeter/millimeter astronomy research, precisely measuring blackbody radiation. The study will include information relating to the technologies used by the Atacama Large Millimeter/submillimeter Array (ALMA) to measure light at these wavelengths. Many interdisciplinary branches in the astronomy field deal with the universe's physical, chemical, and theoretical spectrums. We will concentrate on observational astronomy for this research, which deals with collecting data concerning the observable universe.

a. Electromagnetic Spectrum

This section is tailored explicitly to the different categories of electromagnetic radiation that exist in the physical universe. The standard electromagnetic spectrum comprises seven regions, from longest wavelength to shortest: radio waves, microwaves, infrared, optical, ultraviolet, X-rays, and gamma-rays. For our research, we will concentrate on a specific region found at the end of the microwave frequency region and the start of the infrared frequency region. Here we can discover terahertz radiation, also known as submillimeter radiation ranging from 100 GHz and 10 THz (Terahertz Properties, n.d.). We will explore why this region is vital to present submillimeter/millimeter astronomy applications.

i. Understanding of the Electromagnetic Spectrum

Many objects in space emit and receive electromagnetic radiation, making for crucial information in observational astronomy about our universe. One branch of observational

astronomy works by measuring the millimeter and submillimeter band light from vast cold clouds in interstellar space. We know that light can either behave like a photon particle or a wave of photons, depending on external boundaries (Crockett, 2019). To understand this better, we can first explain the different light spectrums and how they are quantized. Being that light can be modeled as an electromagnetic wave, it has a measurable frequency (or energy) and wavelength that ranges depending on the electromagnetic radiation. The classification of these electromagnetic waves specifies how light is generated and how it interacts with matter. Electromagnetic radiation can be described as the relationship between wavelength and frequency using the equation below:

$$c = \lambda f \tag{1}$$

where c is the speed of light $3x10^{8} m/s$, λ (lambda) is the wavelength, and f is the frequency. For an electromagnetic wave, the wavelength (in meters, m) can be determined by measuring the distance of the crests. The frequency (in Hertz, Hz) is the number of waves that occur in a certain period. This connection can be better illustrated in (Fig. 1), which shows how the two quantities are inversely proportional; for example, a shorter wavelength means a higher frequency and vice versa.

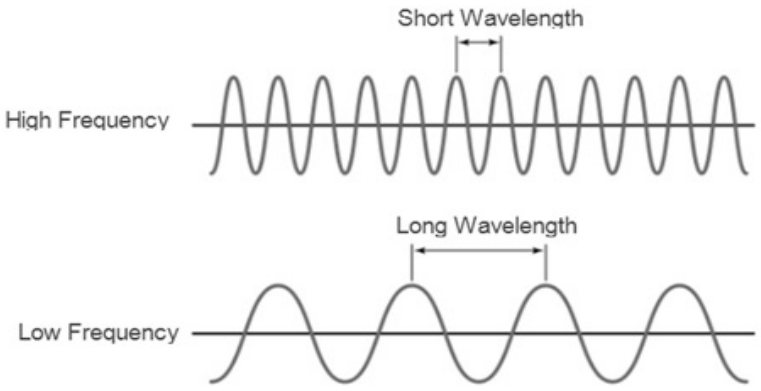

Figure 1. Wavelength and Frequency relationship. link

By this equation (1), it is clear that electromagnetic radiation moves at the speed of light regardless of the wavelength and frequency values. This radiation propagates through space and interacts with matter in different ways. At first, scientists could not understand precisely how electromagnetic radiation interacts with matter since it was known to be a massless property. It wasn't until Max Plank started understanding the properties of blackbodies and their characterizations relating to electromagnetic radiation. His findings eventually led to the discovery of light's elementary particle, the photon, which is absorbed or emitted by atoms or molecules and transmits their electromagnetic energy (Encyclopedia Britannica, 2020). For a body in thermodynamic equilibrium it emits to its environment the same amount of energy it absorbs from this environment. This proportionality is because energy is quantized, meaning that the total energy emitted or absorbed gets transferred in energy packets known as quanta. Planck's equation (2) indicates that this change in energy is directly proportional to the frequency of emitted or absorbed photons.

$$E = hf \tag{2}$$

Here E is the energy of the photon (Joules, J), f is the frequency of the photon (Hz), and h is Planck's constant $6.63\ x\ 10^{-34}\ J \cdot s$. This constant essentially describes the behavior of particles and waves on the atomic scale (Encyclopedia Britannica, 2021). A higher frequency causes a photon with a shorter wavelength and greater energy. In comparison, a lower frequency causes a photon with a longer wavelength and lower energy. To better understand this relationship, we can look at the (Fig. 2), which shows the various types of electromagnetic waves categorized according to their wavelengths and frequencies. The spectrum's classifications go from shorter wavelengths to longer wavelengths: gamma-ray, x-ray, ultraviolet, optical, infrared, microwaves, and radio waves. Shorter wavelengths are associated with radiation damage and

ozone depletion, while longer wavelengths are associated with cell phone use, communication, and heating.

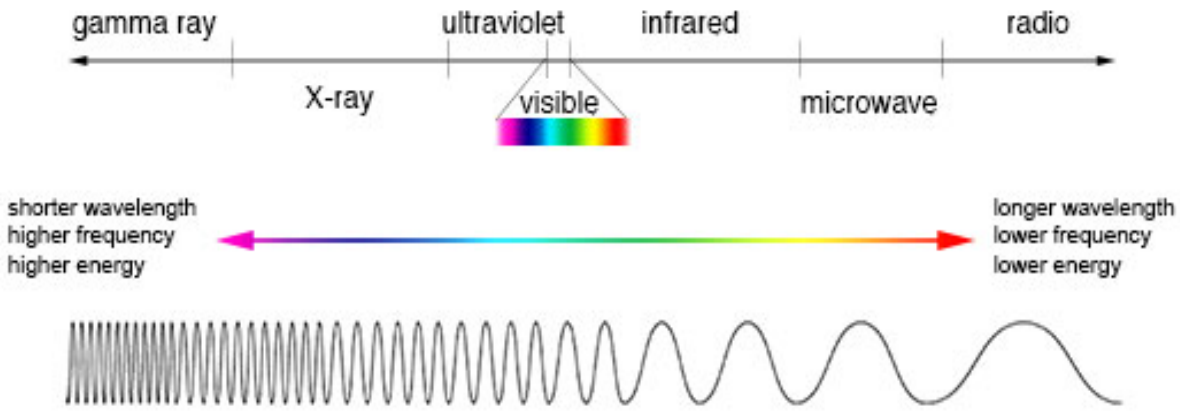

Figure 2. Comparison of wavelength, frequency, and energy of the EM spectrum.

(Credit: NASA's Imagine the Universe link)

These relationships are essential to understand, specifically when dealing with blackbodies emitting photons at terahertz frequencies. This type of frequency has proved to be crucial for astrophysical research potential using spectroscopy technologies and radioastronomy. The following chapters will explain blackbody and terahertz radiation and its known use for gathering astronomical data for celestial bodies.

ii. Blackbody Radiation

A blackbody is an ideal object that obeys the thermal radiation laws, and it distributes radiant energy according to its wavelength. In the vacuum of space, the energy photons carry depends on the temperature of the blackbody emitting it. The temperature emitted by a blackbody determines the wavelength at which the radiated energy is at its peak (Fig. 3). Fundamentally, electromagnetic waves emitted by a blackbody are called blackbody radiation. Our understanding of this relationship between the temperature of a blackbody and the

wavelength at which it emits the most light can be characterized using Wien's Displacement Law. This radiation law states that the wavelength of peak emission of blackbody radiation is inversely proportional to the temperature of the emitting object. Wien's equation (3) can be written as the following, where λ is the wavelength peak, b is the constant of proportionality, and T is the absolute temperature.

$$\lambda = \frac{b}{T} \tag{3}$$

Correspondingly, this information relates to a star's temperature, as it will determine the visible color of the electromagnetic spectrum according to its wavelength. The power emitted by a body in thermodynamic equilibrium, such as a blackbody, is related to a function of its physical temperature (Blackbody Radiation, 2020). The higher temperature a blackbody has the higher energy this body will radiate, and the shorter the maximum emission wavelength.

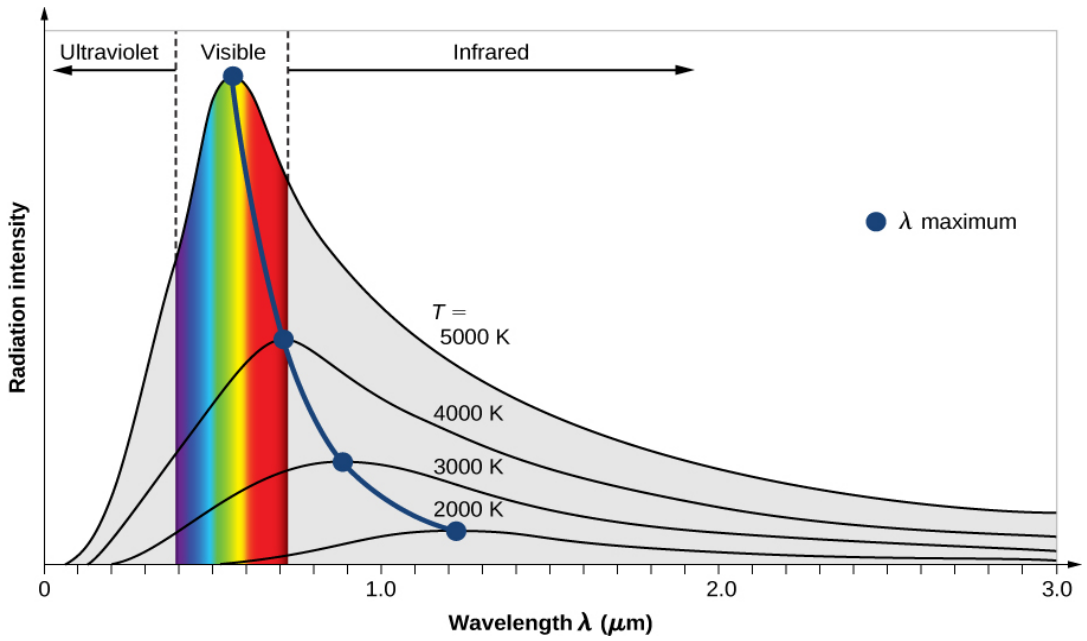

Figure 3. The intensity of blackbody radiation versus wavelength of radiation emitted. link

An example of this relationship is in stars; some stars in our galaxy with low temperatures, like the Sun, display a reddish hue. Another example is the cosmic microwave

background radiation that the universe is bathed in relates to a temperature of 2.7 K that peaks at a wavelength of 1.1 mm. Much of the interstellar medium are remnants of stars and have temperatures around ~10-100 K and emit radiation in the millimeter-wave/submillimeter-wave/THz electromagnetic band. In radio astronomy, the power received by a telescope is give by:

$$P = kTB \tag{4}$$

where P is the power emitted by the blackbody, k is Boltzman constant, T is the temperature of the blackbody and B is the bandwidth of the receiver. This equation (4) also relates to the thermal noise power of a filtering receiver, such as those used in spectroscopy research. The noise temperature is used to present how much thermal noise is generated from active or passive devices in the receiving systems, much like a satellite or antennas (Iida, T., & Wakana, H., 2003). The noise temperature values must be as low as possible to improve the performance of the receiving systems.

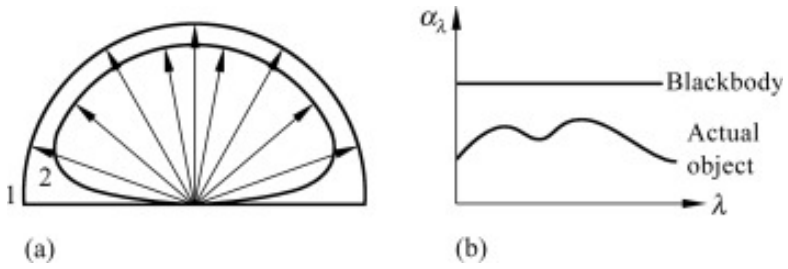

Figure 4. Radiation and absorption of a real body compared to a blackbody. link

As mentioned before, according to Planck's Law of Blackbody Radiation, a blackbody radiates and absorbs energy uniformly in all directions (Fig. 4). When comparing a real body to a blackbody, we can see that a real body does not obey the laws of surface thermal radiation. This is because a real body's radioactivity and absorptivity characterizations are dependent on its geometric structure (Zhang, Y., Li, Q., & Zhou, H., 2016). However, unlike a real body, a

blackbody's energy is radiated and absorbed uniformly through space, obeying Planck's Law regardless of geometric form. The radiation entering the blackbody is balanced by the radiation leaving it at thermodynamic equilibrium. Using this equation (5), we can explain the spectral density of electromagnetic radiation emitted by a blackbody in thermal equilibrium. Planck's Law for the energy radiated by a blackbody can then be written in terms of:

$$I_f = \frac{2hf^3}{c^2}\left(\frac{1}{e^{hf/kT}-1}\right) \quad (5)$$

where I_f is the spectral specific intensity $Wm^{-2}sr^{-1}Hz^{-1}$, h is Planck's constant, f is frequency, k is Boltzmann's constant $1.38\ x\ 10^{-23} J\ \cdot K^{-1}$, T is the blackbody's absolute temperature (K), and c is the speed of light.

We studied a variety of equations and deduced that these equations help us better understand the concepts behind the electromagnetic spectrum. Each relevant mathematical principle was then related to research regarding blackbody radiation to see how these are applied. The ultimate goal of these efforts is later used and explained in the Methodology and Results chapters of this paper.

b. ALMA

The Atacama Large Millimeter/submillimeter Array (ALMA) is an astronomical project located in the Atacama desert in Chile. Its construction began in 2003 and now it operates at 2900 meters above sea level alongside 21 other countries in Europe, North America, East Asia, and Chile (Factsheet ALMA, 2022). It is an array composed of 66 antennas that simultaneously work together to point at the same point in the sky. A single one of these antennas weighs 100 tons and costs over 10 million dollars (Factsheet ALMA, 2022). The antennas' meticulous

design and 12-meter diameter receive astronomic signals deep within space and process them appropriately. First, the measured analog signals get converted to a digital format and transported to the main building. Once in the main building, a supercomputer later correlates the signals and generates data analyses relating to the source of that signal. ALMA allows astronomers to gather data that has traveled years through space and reached us on Earth by these means.

Figure 5. The array of ALMA antennas in the Atacama desert. link

ALMA is the most outstanding astronomical project concentrating on radio signals received from space. These signals are found between the far-infrared and radio waves in the electromagnetic spectrum. The radio telescopes at ALMA allow astronomers to study the colder distant parts of the universe. In the electromagnetic spectrum, infrared and radio waves have longer wavelengths meaning that this signal is relatively weak compared to the others (Fig. 2). For ALMA to pick up these weak signals, they use a technique known as interferometry by using several antennas to allocate data from a single coordinate. Interferometry allows radio astronomers to combine signals from many antennas to learn more about our universe and increase the angular resolution. The research regarding signals from cold space allows ALMA to untangle mysteries about our universe and its evolution.

Understanding the technicality of the ALMA antennas was a crucial process for our modeling of a blackbody source. Since this research proves critical to understanding our universe, its properties, and what we can expect in the future, we plan to dive deeper into this knowledge. An important step is becoming familiar with the technicality of the antennas and the millimeter/submillimeter range they operate at.

i. How ALMA Antennas Operate in the Millimeter/submillimeter Range

Millimeter/submillimeter (mm/sub-mm) astronomy is a relatively new branch of observational astronomy dating back to the 1960s. The mm/sub-mm band refers to the electromagnetic spectrum of light, specifically in the molecular universe. It contains spectral and spatial information on the cosmic background, very distant newly formed galaxies, and the early stages of star formation within gas clouds in our universe (Wolstencroft, R. D., & Burton, W. B., 2012). Crucial information is available in the specific band of electromagnetic radiation that exists in the universe. We need accurate antennas and sensitive receivers to make precise measurements from Earth. To interpret the data collected, a further understanding of atomic and molecular physics and interstellar chemistry is also necessary.

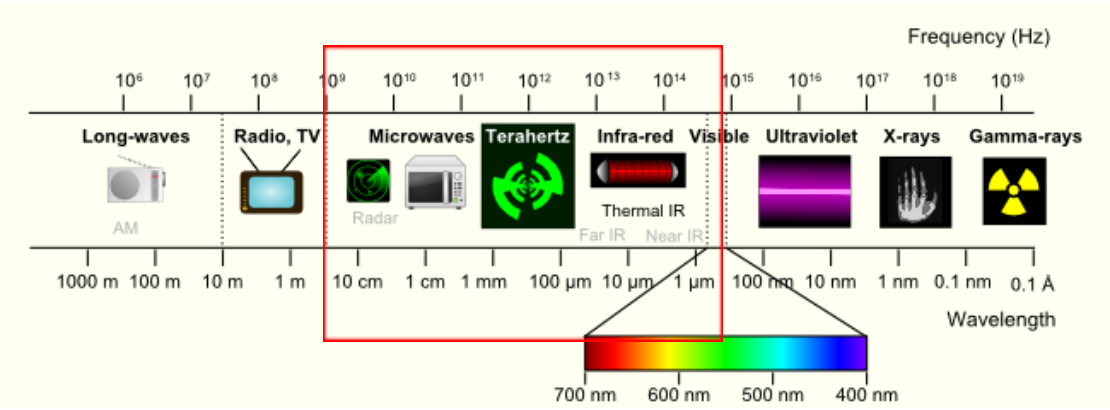

Figure 6. Electromagnetic spectrum with Terahertz region highlighted. link

The terahertz (THz) regions represent the electromagnetic radiation between the

microwave, and the infrared regions, as seen in Figure 6. ALMA operates at wavelengths of 0.3 to 3.6 mm, specifically tailored to research these regions of the electromagnetic spectrum (ALMA, 2022). This range of the electromagnetic spectrum is crucial for studying stars and galaxies; it is also capable of measuring energy emitted from supermassive black holes and stars. The ALMA antennas measure these terahertz radiation signals that reach Earth, using a sophisticated receiving system customized to quantize and correlate this data (Morata, O., & Huang, T., 2017). Ultimately, the data acquired serves a purpose for research and new insights into astronomical and physical phenomena we might not understand.

The array of antennas that ALMA utilizes works in unison to receive signals from the same coordinate in space, where a cosmic object possibly resides and emits energy. Nonetheless, these antennas comprise different types of equipment that serve specific functions for the data to be accurate. Figure 7 shows the setup for a basic radio receive system and the components the data goes through.

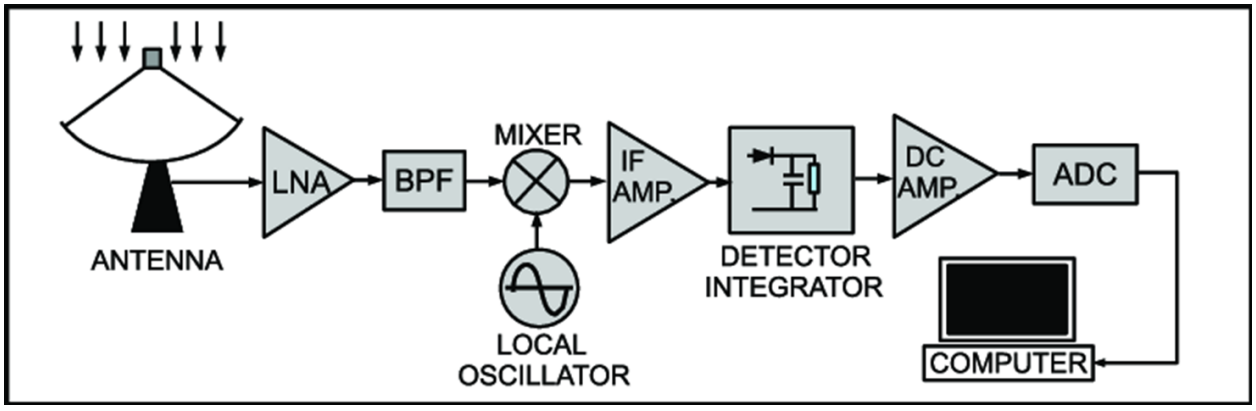

Figure 7. The antenna, low noise RF amplifier (LNA), mixer, local oscillator, IF amplifier, detector, DC amplifier, and data recording computer are shown. link

Once a radiation signal reaches the antenna dish, it reflects onto a mirror mounted at the center. From the mirror, radio signals reflect into a heterodyne receiver located inside the

antenna. The heterodyne receiver is an essential component since it measures both the amplitude and phase of the signal. The radio frequency signal passes through an amplifier to enable the input signal to control an output signal (APITech, 2022). Here, the incoming radio frequency signal is mixed with a signal from a local oscillator. The local oscillator produces a lower fixed frequency signal called intermediate frequency. The intermediate frequency amplifier changes the frequency levels that are difficult to tune and unstable, making the signal accurate. Next, this signal goes through a DC amplifier to fine-tune low frequency and DC signals. Astronomers must keep the signals collected by ALMA at a temperature of 4 Kelvin (-452 Fahrenheit) to prevent introducing noise to the signal reading (Moskowitz, 2013).

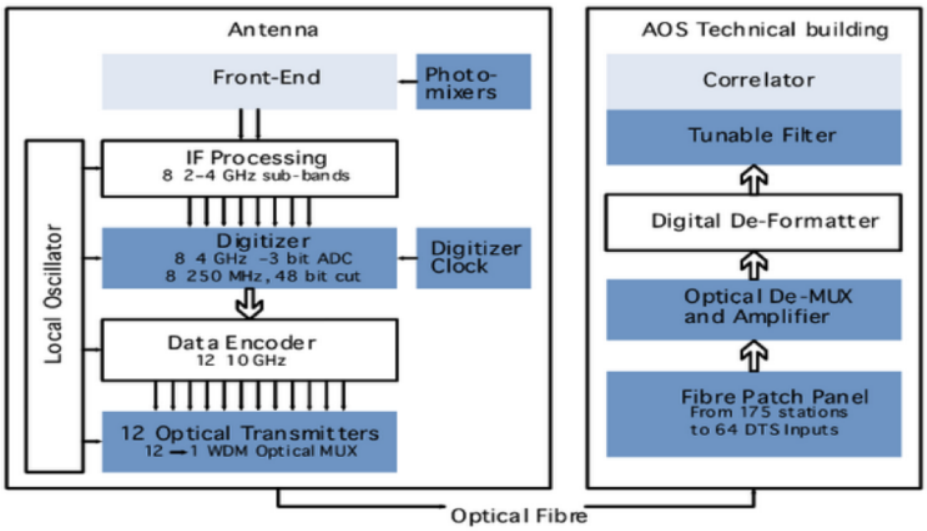

Figure 8. ALMA signal processing and data transfer. link

The analog signals received by the antennas go from converting to digital signals. This procedure is achievable by the front-end electronics installed on each antenna. The analog data gets converted to digital data and sent to the Array Operations Site (AOS), which is at ALMA's back-end systems. Fiber optic cables then transmit the digital signals to the AOS Technical Building for better debugging and analysis (ALMA, 2022).

c. Understanding Black Body Radiation Data

In this chapter, we apply our understanding of the electromagnetic spectrum and blackbody radiation measured by ALMA. The objective is to correlate blackbody radiation and physical celestial objects. We can associate the data mining processes ALMA uses to measure blackbody radiation by exploring the relationships between these concepts and a particular star such as Betelgeuse. The goal of this is to study the properties of stars while identifying future tangible modeling of a blackbody source.

i. Hertzsprung–Russell diagram

The Hertzspeung-Russell diagram, also called the HR diagram, was developed around 1911 by Danish astronomer Ejnar Hertzsprung and U.S. astronomer Henry Noris Russell. The HR diagram is a scatter plot used to classify stars based on their temperature and luminosity. The spectral types (or temperatures) range from the sequence OBAFGKM, running from the hottest stars to the coolest (Hertzsprung-Russell Diagram, 2022). This factor is plotted against the star's absolute magnitude (or luminosity), which is calculated using the star's apparent magnitude. This measurement is the magnitude the star would have if it were viewed from Earth, a distance of precisely 10 parsecs. It's used to compare the brightness of stars to sort them in the HR diagram properly. This diagram provides astronomers with important information about the stars detailing their diameter, mass, age, and evolutionary stage (Hall, J. C., 2018). Since stars are constantly evolving and alternating these properties, the HR diagram serves as a measure for predicting the star's evolutionary phase.

ii. The life cycle of stars

Stars have been an essential contributor to human evolution since we began to study them and how they behave. Ancient astronomers, dating back to 1000 BCE, have recorded the motions of these celestial bodies relying on minimal machinery compared to our present. These observations made in the past have helped societies develop technologies such as determining the periods of a calendar to keep track of time (Buitenen, J. et al., 2021). The advancement of astrometry has provided humans with a greater knowledge of the universe and its cycles of evolution. Our attempts to study these cycles will bring us closer to understanding how the universe began, dating back to 13.8 billion years ago (Gohd, C., 2021).

The stars being born are created from the surrounding matter in the space between other celestial bodies, which we call the interstellar medium (ISM). The ISM comprises interstellar gas partly of neutral atoms and molecules and charged particles, such as ions and electrons (Herbst, E., 1995). The chemical composition of this interstellar medium is mostly gas, such as hydrogen and helium, along with dust particles made up of carbon, ice, or iron compounds (Ehrenfreund, P., & Cami, J. (2010). Stars are formed in these clouds of gas and dust called nebulae, also known as stellar nurseries. These clouds are home to very dense material that eventually folds into itself due to gravity. A star is only formed when these materials become hot enough for the hydrogen nuclei to fuse to make helium; otherwise, it remains a prostar. This step is called nuclear fusion, where two lightweight atoms are forced together to form a heavier atom, producing a lot of energy (Stars, 2022). The energy produced by this nuclear reaction is located at the center (or core) of the star, which allows it to shine brightly. Once the star can give energy as light and heat, it belongs to the main sequence stage (Stars, 2022). Following this, essentially, the size of the star will dictate its exact lifetime. More giant stars use up their fuel quickly,

making them last a few hundred years. Whereas smaller stars use fuel more slowly, making them last for several billion years. The star eventually reaches the final phases of its life once it runs out of hydrogen to power its nuclear reactions, meaning that it runs out of energy to produce heat. Every star evolves to this red giant phase (helium fuses into carbon), depending on the star's mass determines which of the following phases it follows from there. Smaller stars go through the planetary nebula phase, where the star produces stellar winds, which throw off the outer layers into its surroundings. Eventually, this low-mass star runs out of fuel and becomes a white dwarf, the bright, hot, dense core which remains after a planetary nebula (NASA, n.d.). On the other hand, massive stars follow a different final phase that causes an explosion leading to two different outcomes: neutron star or black hole. A supernova is a massive explosion caused by gravity pulling all the material in the star towards the middle, collapsing the star to its core. During the explosion, the core collapses down to create either a neutron star or a black hole (NASA, n.d.). The remnants of the blast eventually drift into space and become part of a nebula, essentially recycling the elements from the first star to make new stars or celestial bodies.

iii. Supergiant Stars

Supergiant stars are the most luminous and massive objects in the universe, with initial masses above 8-10M (solar mass). These stars are enormous compared to our Sun and follow different phases in the lifetime of a star. As mentioned before, stars in the supergiant phase emit so much energy that they begin to fuse heavier elements up to iron. Because of their large mass, these stars have very short lifespans of around 3 to 100 million years since they burn their energy faster (Supergiant Stars, 2021). This process feeds the universe with heavier elements as the star begins to collapse due to gravity. Due to this expansion and energy release, supergiant stars start to cool down and drop in temperature. Supergiant stars are found in the top corner of the HR

diagram because of their size, luminosity, and temperature. These stars can belong to two different categories such as blue supergiants and red supergiants. Blue supergiants (BSG) are the hottest and brightest stars in the universe ranging from 10,000 K to 50,000 K in temperature. In the HR diagram, these stars are classified in the O or B spectral type and are found along the top left corner. On the other hand, red supergiants (RSG) are giant stars in the universe in terms of mass and range roughly from 3,000 K to 4,000 K in temperature (Levesque1, E., 2005). The spectral type for these stars is K or M in the HR diagram and can be found along the top right corner. In the final phases, both stars always explode as a supernova and feed the universe with heavier elements.

iv. Betelgeuse

As part of this experiment, we will be paying attention to data relating to the RSG Betelgeuse to understand the processes of submillimeter astronomy. Betelgeuse, also called Alpha Orionis, is the second brightest star in the constellation of Orion and the tenth most luminous star in the sky (Britannica, 2021). Its distance from Earth is approximately 500 to 600 light-years (ly) and has an apparent magnitude varying between +0.0 and +1.6. The star is approximately 767 million miles in diameter (12M solar mass) and between nine and ten million years old (Briggs, A., 2020). The size and age of the star set it at a spectral type of M1-2 in the HR diagram. Understanding stars such as Betelgeuse is essential for us to pinpoint important events that shape the evolution of our universe. Eventually, all supergiant stars, including Betelgeuse, will die in an explosion, causing a supernova. When stars reach this point of exhaustion, they tend to drop both in temperature and luminosity; these are usually identifiers of the stars' foreshadowed death.

Although for some stars, these identifiers aren't usually enough to appropriately determine when the star will commence its demise. We call these variable stars, and they aren't unusual; Betelgeuse is one of them. Variable stars are stars whose brightness (or apparent magnitude) varies over time, caused by different factors (Briggs, A., 2021). For instance, something could block the light emitted by the star, such as a dust cloud or even an orbiting celestial body. Another reason for varying brightness is the star's periodical change in luminosity, where it swells and shrinks. Because of these facts is why it's vital for us to closely observe Betegeuse's behaviors to understand better RSG and the role they play in our evolution once they die.

3. Methodology

In efforts to fulfill the project goal of analyzing data publicly available at the ALMA site to understand other technologies that focus on the spectroscopy of the interstellar molecular clouds in millimeter and submillimeter wavelengths, we set the following objectives:

1. Understand relevant physical equations relating to terahertz radiation to understand further interferometer detection of blackbody radiation such as technologies used by ALMA.
2. Become familiar with various lab equipment and perform appropriate device measurements to calibrate devices and further understand how these apply to the millimeter and submillimeter astronomy.
3. Design an experiment to simulate how ALMA collects data from the universe on a smaller scale to become familiar with the process.

Objective 1: Understanding Blackbody Radiation Measurements

To accomplish this first objective, we conducted a literature review on radiometric quantities and the process of measuring them. This review meant studying principles such as Planck's quantum theory and the derivation of the blackbody radiation law. Our efforts in modeling blackbody sources included understanding the properties of microwave radiometric systems, noise temperatures, and terahertz astronomy. This resulting extent of literature review served as a template to gather device measurements for our second objective. Relevant equations can be found in the Background section of this paper.

The most important equations to be used in experimentation are the ideal total-power radiometer (6). This equation describes the relationship between the antenna temperature T_A and

the receiver input noise temperature of the receiving system. Where $T_{SYS} = T_A + T_{REC}$, B is the signal bandwidth, τ is the time constant and ΔT is the smallest change detectable by the measurements in the system, otherwise called the radiometric sensitivity of the system.

$$\Delta T = \frac{T_{SYS}}{\sqrt{B\tau}} \tag{6}$$

A linear relationship between the unknown antenna temperature T_A and the measured output voltage $\overline{V}_{out}$ can be described by the following equation:

$$T_A = \frac{\overline{V}_{out}}{G_s} - T_{REC} \tag{7}$$

Where G_s is the overall system gain factor which is the relationship between the magnitude of the input to the magnitude of the output signal. By incorporating the effect of both noise and gain variations to the radiometer sensitivity expression of the total-power radiometer, we can deduce the power temperature noise power of a receiving system using equation (4).

Objective 2: Become Familiar with Apparatus Used for Experimentation

For the following experiments, we performed tests in the 5G / 6G mm-Wave Lab room. Before setting up a complete experiment, it was essential to become familiar with various pieces of equipment that would be used and perform some calibrations of equipment to ensure they were functioning correctly. A primary goal for this project was to gain additional hands-on experience using different pieces of lab equipment. With this in mind, the various components used for experimentation included a radio frequency signal generator, an oscilloscope, a

heterodyne receiver, various amplifiers, a detector, an optical chopper, an analog lock-in device, and equipment used for data collection.

The first piece of equipment introduced in this project was a Microwave Signal Generator, also known as a synthesizer. This device "is to generate a signal with known characteristics: frequency, amplitude, modulation" (ElectronicsNotes.com, accessed 2022). The device, shown in Figure 9, was used to output a specific frequency and amplitude used in two different parts of the experiment. Before the final experimental setup assembly, the radio frequency signal was used to ensure we calibrated the detector correctly.

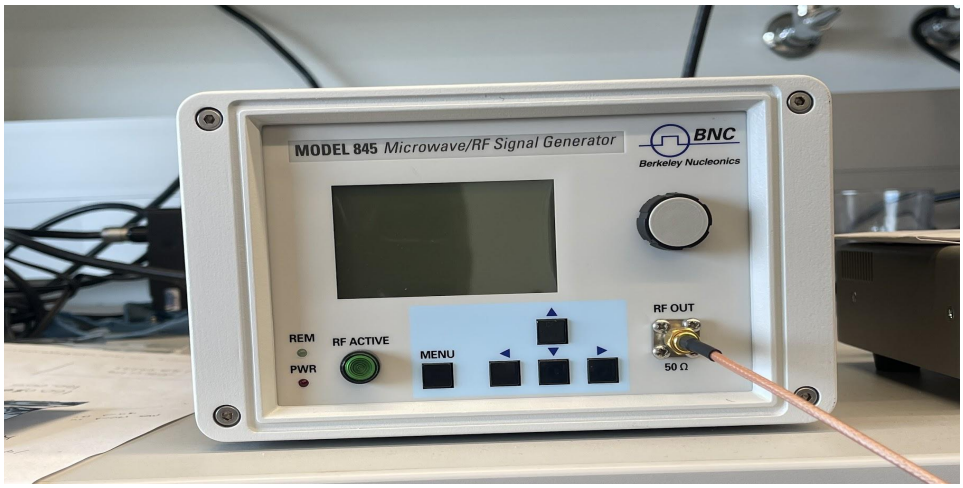

Figure 9. Microwave/Radio Frequency Signal Generator.

The power detector operates at 50 Ohms, with a 10 to 8000 Megahertz (MHz) frequency range. The device provides low noise with a wide bandwidth across varying input powers. The synthesizer must be powered at about 5 volts and 120 milliamps to operate the detector. An image of the power detector can be found in Figure 10. This test was done using the amplifier power supply seen in Figure 11. In order to become familiar with how the radio frequency signal generator operates, we calibrated the power detector over varying input powers at different frequencies.

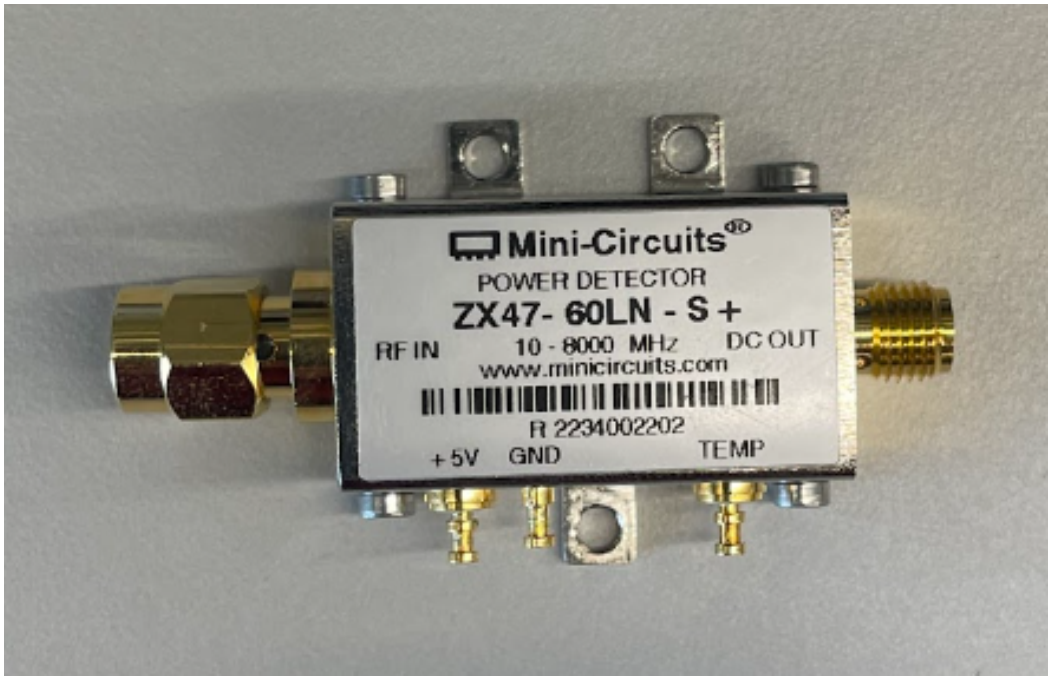

Figure 10. Power Detector.

Figure 11. Amplifier Power Supply.

Figure 12. Oscilloscope.

We used an oscilloscope to track the detector's output voltage. An image of the oscilloscope can be seen in Figure 12. It can track this voltage over time and the USB can record the output from the oscilloscope. The set-up used to calibrate the detector was reasonably straightforward. The radio frequency signal generator is connected to the input side of the detector using SMA cables. The output of the detector is connected to the oscilloscope using another SMA cable. In order to verify the detector was behaving as expected, calibration was conducted at various frequencies and decibel (dBm) power levels. The output voltage at varying power levels and frequencies matched the specifications sheet provided by the company in Figure 13. The bandwidth of the detector was approximately B~8 GHz and from the figures, one can observe the sensitivity is slightly less at 8 GHz. Experimental data is provided in Figure 14 and was very closely related to the spec sheet. Data from the experiment can be found in

Appendix A. The detector was the overall limiting device in the bandwidth of the system related to Eqs. 4 and 6 and limited and limited the sensitivity of the system.

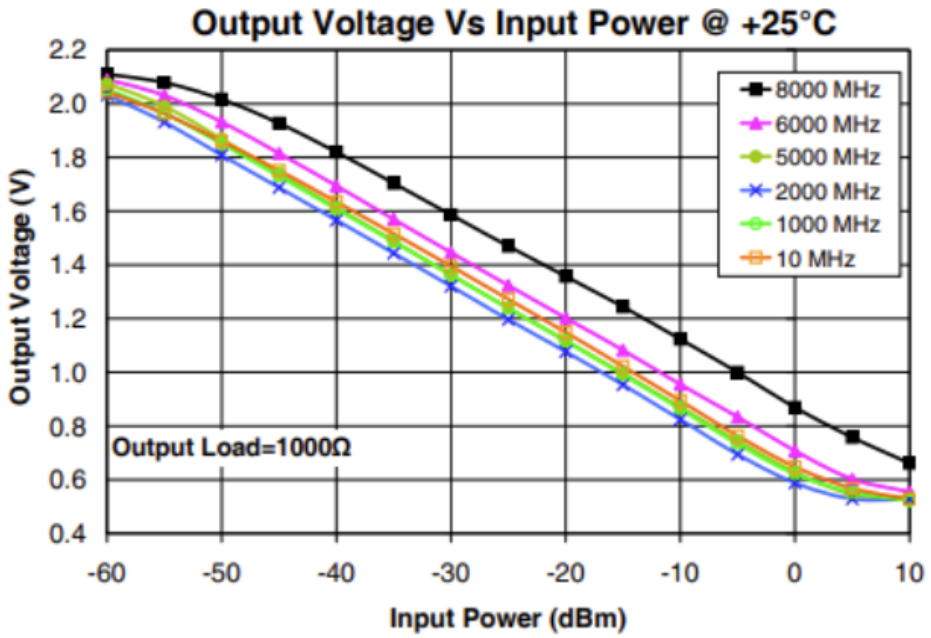

Figure 13. Specifications sheet for Power Detector.

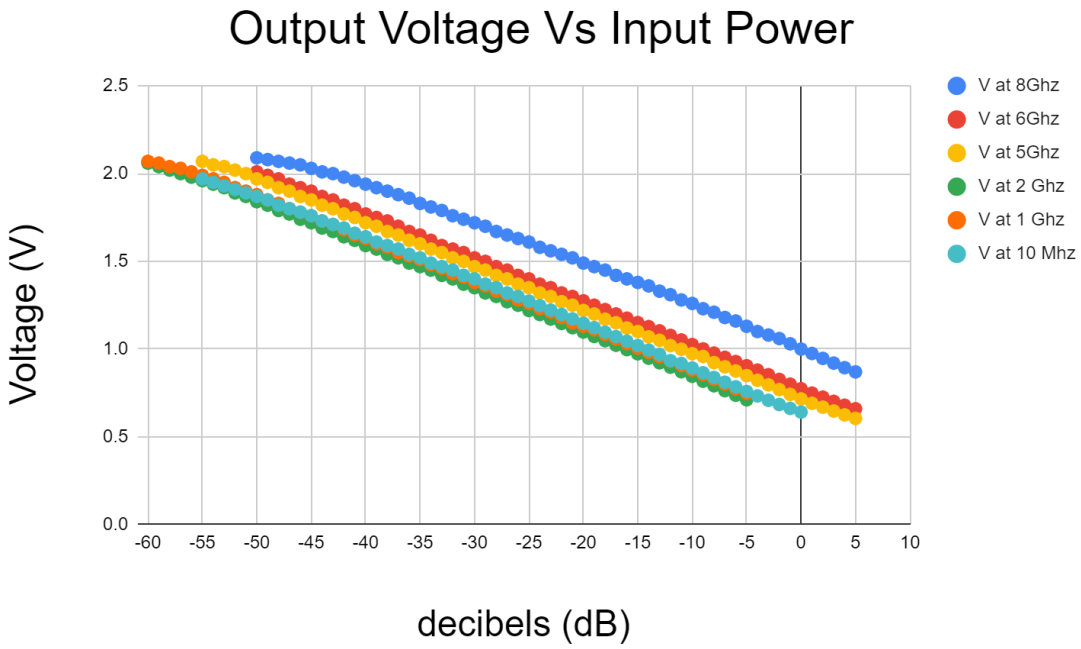

Figure 14. Output Voltage Vs. Input Power Graph of Calibration Test for Power Detector.

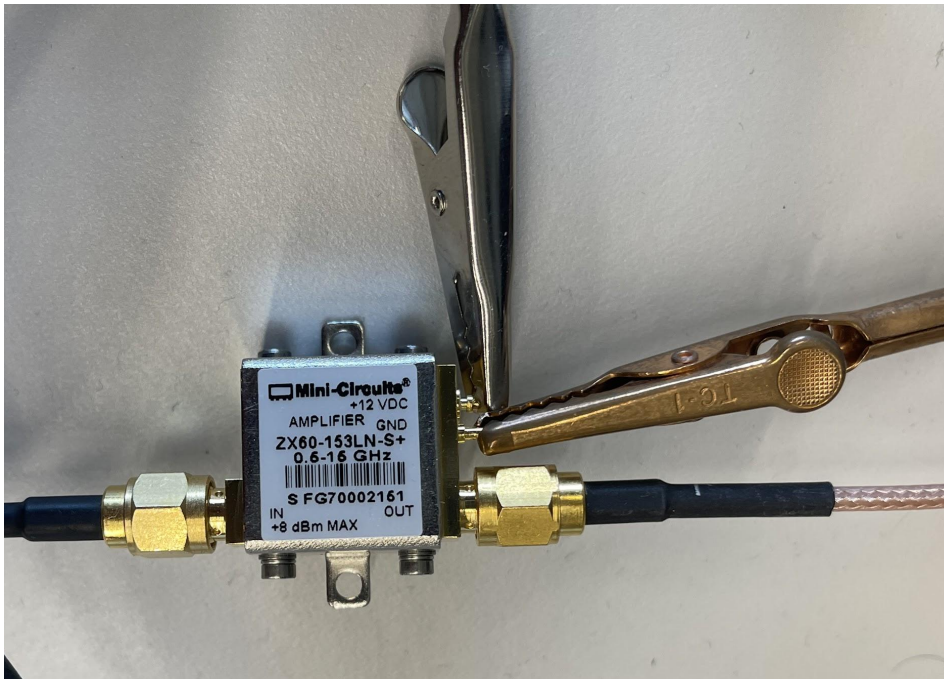

Figure 15. Mini-Circuits Amplifier

Another critical component in the experimental setup was an amplifier in Figure 15. We used this device to boost the signal output from the heterodyne receiver. The amplifier used in the official experiment operated at 12 volts and was run in parallel before the detector. Another passive detector was used in a trial of the investigation, but the device was not sensitive enough to provide valuable data. The passive detector can be seen in Figure 16. This had a bandwidth of 26 GHz, but did not seem to be sensitive enough to detect the signal from the heterodyne system.

Figure 16. Passive detector tested but not used.

The following device is the centerpiece of the experiment. The heterodyne receiver, pictured in Figure 17, is a device that can track radiation from the environment and convert thermal energy into power. The golden horn seen at the front left of the heterodyne receiver is used to monitor radiation and allow the receiver to get input. The heterodyne receiver was a piece of equipment that very little was known about for the project's scope. Its internal workings were unclear, and the device was something our team was to become familiar with and how it operates. What was known about the heterodyne receiver is that it was connected to the receiver power supply, shown in Figure 18. The bandwidth of the Intermediate Frequency (IF) was 20 GHz.

Figure 17. Heterodyne Receiver with Horn Antenna.

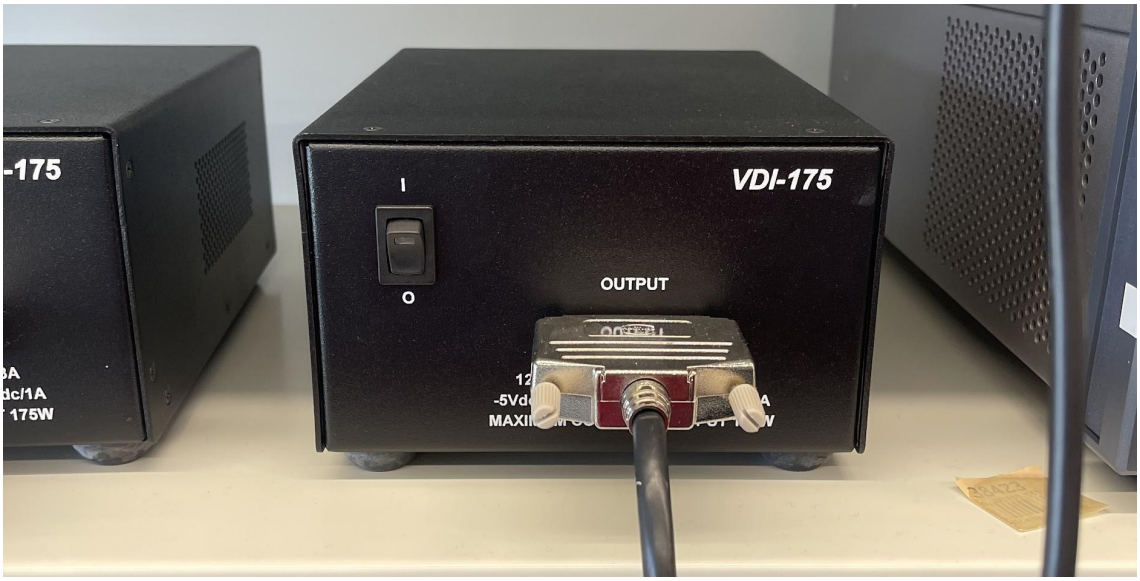

Figure 18. Heterodyne Receiver Power Supply.

The following device to be used later in the experiment was an optical chopper. The chopper is a blade connected to a power source that controls the rotation rate. The blade has slits that allow signals to pass through solid segments that block light. For the purpose of our experiment, a blade was used with equal spacing of open and blocked slits. The optical chopper itself is pictured in Figure 19, and the power source that controls rotation is shown in Figure 20.

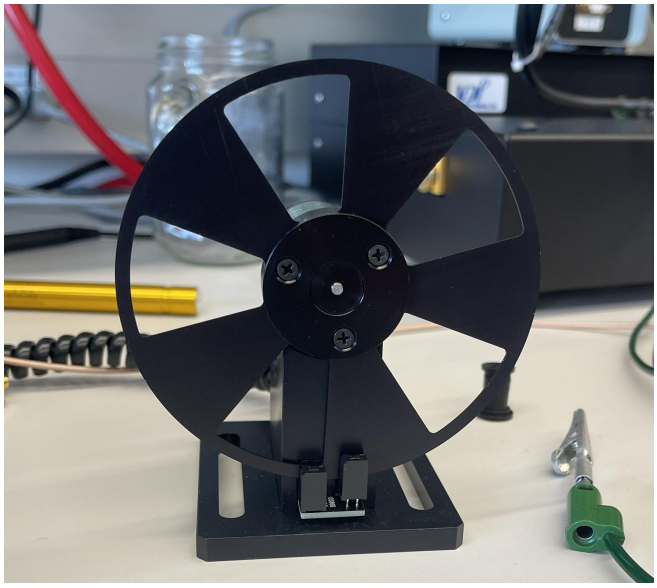

Figure 19. Optical Chopper

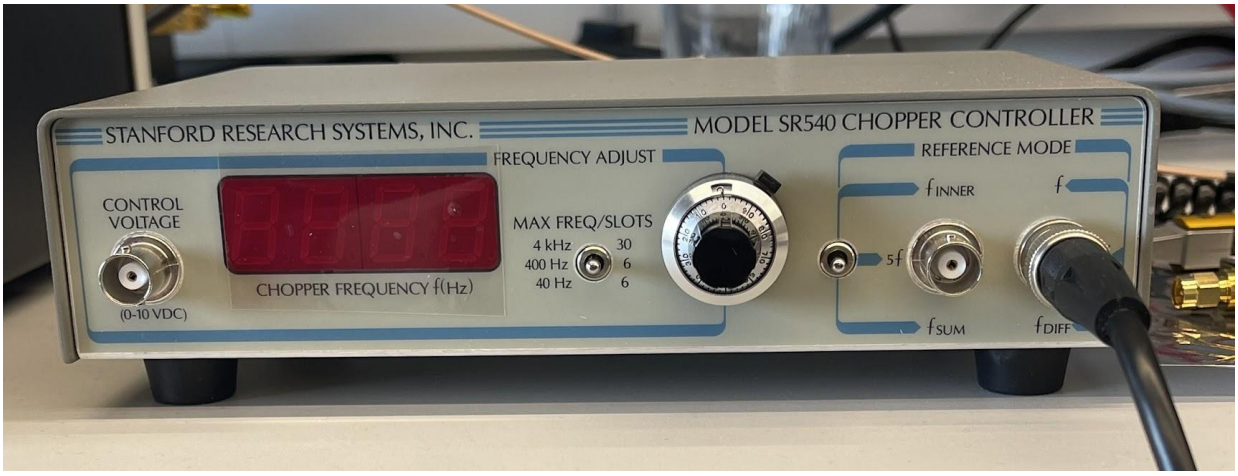

Figure 20. Optical Chopper Power Supply

Another instrument used in the experiment was the analog lock-in device in Figure 21. The lock-in device works by taking in a signal; for the investigation, it would be the output from the detector and comparing it to a frequency. The frequency to be compared would be the optical chopper, which is set to some rotation speed. By knowing the frequency of the chopper, the lock-in can integrate over a specified time period to remove noise and only return the signal from when light passes through the chopper or when it does not (PhysicsOpenLab, 2022). The signal returned is a DC voltage, which could then be passed to the oscilloscope to view. For experimental purposes, the output from the x-axis was split to go into the DAQ and the oscilloscope, and the y-axis output was fed to the DAQ. In order to limit the variation on the y-axis, the analog lock-in amplifier could be phased to have all the output go to the x-axis.

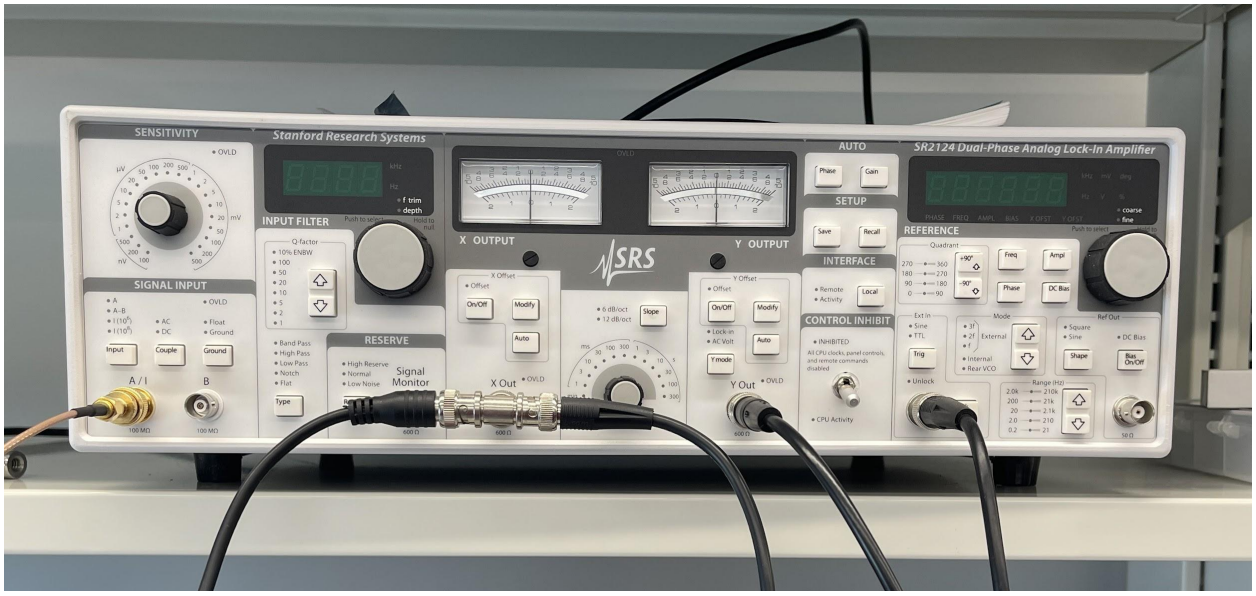

Figure 21. Analog Lock-in Device.

The final two components involved in the experiment were used for collecting data. A DAQ from National Instruments was used to receive data from the output of the analog lock-in amplifier over two channels, the x out and y out. The DAQ would measure the voltage outputs at

a data retrieval rate determined by a Labview program. An image of the DAQ can be found in Figure 22.

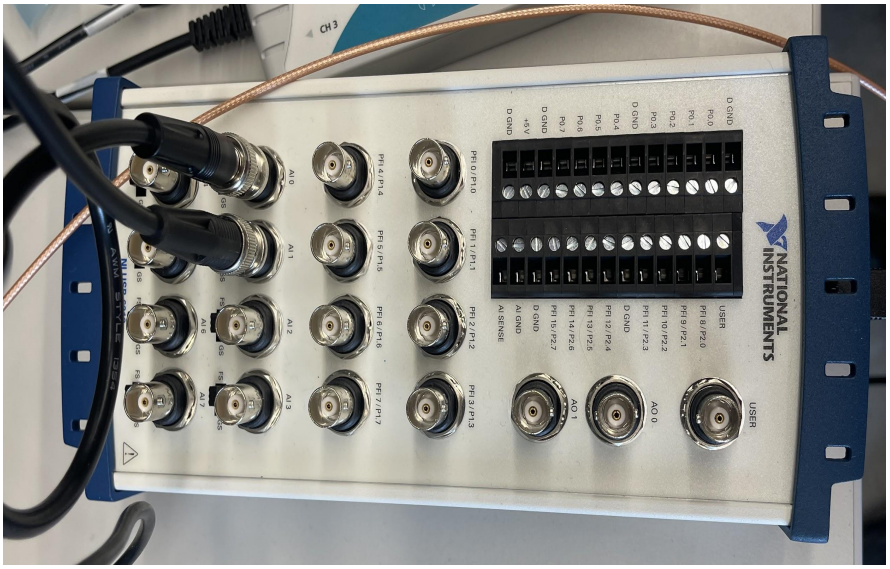

Figure 22. DAQ Assistant.

The final instrumentation used for data acquisition is a Vernier LabQuest Device. This device was operated through a Vernier application where data collection rate and duration could be specified. For our experiment, two temperature probes were connected to the LabQuest, that could be used to monitor the temperature of the environment and of hot water that would be used for radiation. An image of the LabQuest device is provided in Figure 23.

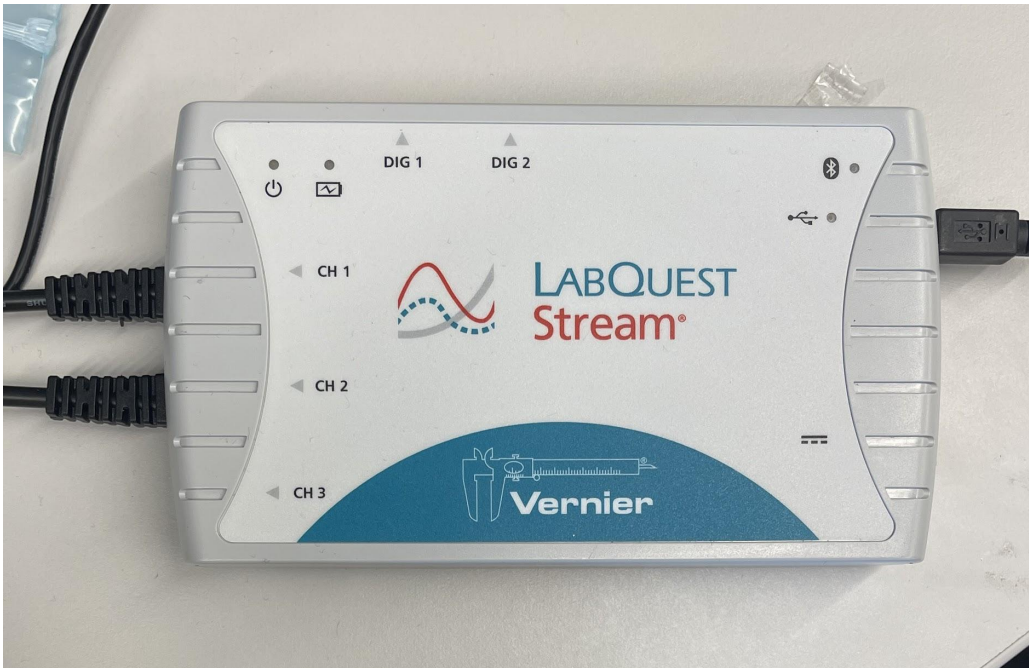

Figure 23. LabQuest Device.

Objective 3: Experimental Design

The design and functionality of the ALMA satellite can be found in the Background chapter (Fig. 7). A heterodyne receiver was necessary to design an experiment using a similar apparatus. This device had not been used in the physics laboratory at WPI, and little information was known. The receiver's operating frequency was 140 to 220 Gigahertz and was powered electronically. Attached to the front of the receiver is a small horn used to measure the radiation of the surrounding environment. We connected a radio frequency mixer to the heterodyne receiver to replicate this setup. After researching the heterodyne receiver, we learned that the internal components had a frequency multiplier of 18 times that of the source input. In order to be within the operating frequency of the receiver, a frequency of 8.888 Gigahertz was used out of the radio frequency mixer. This set the center frequency of the local oscillator to 160 GHz, so

the thermal band from 150-170 GHz (20 GHz bandwidth) was the output of the heterodyne receiver.

For the experiment, a mason jar was used with boiling water to simulate a blackbody. This addition meant that the thermal energy detected by the heterodyne receiver would be fairly weak compared to an actual blackbody source or even iron heated above 500 degrees celsius. An image of the mason jar is provided in Figure 24 below.

Figure 24. Mason Jar used as a blackbody source.

The heterodyne receiver takes in thermal energy over the 140-220 GHz operating band and compares it to an internal reference frequency, called the local oscillator, to create a beat that is outputted from the receiver. In this case, the local oscillator was at 160 GHz. In this way, the heterodyne receiver "works like a radio for light," and output can be measured in different ways

depending on the desired end goal (Science Direct, 2008). For this experiment, the goal was to create a design similar to ALMA's to become familiar with how their data is collected. Thus, for our experiment, the output of the heterodyne receiver was directed to the amplifier, active detector, and lock-in amplifier and the output was a voltage proportional to the received thermal power.. However, since our blackbody source was fairly weak, the voltage output change was not observable without the amplifier. To increase the sensitivity, the amplifier was added to the system to boost voltage output. The detector used had an operating frequency between 10 megahertz to 8 gigahertz, which was sufficient as the output frequency from the heterodyne receiver is 20 GHz.

Being confident that the amplifier and detector were behaving correctly, the setup was nearly complete. The detector's output was then attached to an oscilloscope, which was used to monitor the voltage level. By waving a hand in front of the horn, an increase in voltage could be seen on the oscilloscope. However, our team later realized this was not because our experiment worked properly. The first issue was that energy from the local oscillator 'leaked out' and would be reflected directly back into the horn if the angle of the object's surface was normal to the direction of the horn. The next and most significant issue was that the receiver, amplifier, and detector produced high noise levels. This issue meant that the signal on the oscilloscope was essentially the sum of noise levels from each of these devices. In order to remedy this issue, an optical chopper and an analog lock-in device were introduced to the experiment.

An optical chopper is a thin wheel that works by spinning at a set frequency. The wheel has portions of metal with slits that allow light to pass through. In this sense, the optical chopper essentially created a signal of light passing through and light getting blocked. When combined with the analog lock-in device, that signal can be used to reduce the noise from other devices in

the system. The lock-in can integrate over a set time period, τ, resulting in the system's noise being reduced as shown in Eq. 6 , and instead, only the signal created from the optical chopper will remain. Thus, the hot water source was placed directly behind the optical chopper so that the receiver would either be detecting radiation from the hot water or room temperature. This signal would then be converted to voltage, and as the hot water cooled to room temperature, the signal strength would decrease, and voltage would decrease as well. A complete setup of the experiment can be seen in Figure 25.

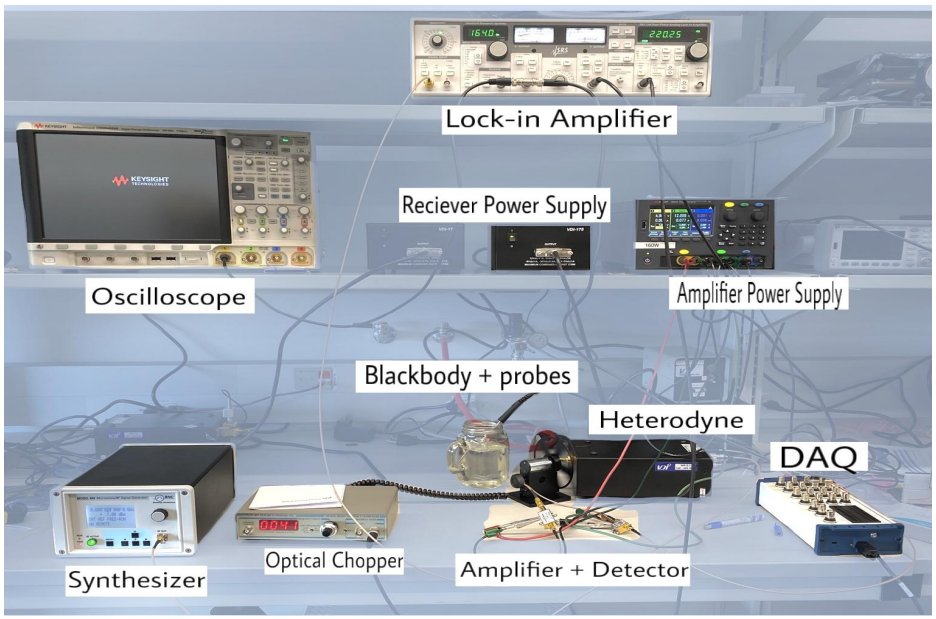

Figure 25. Final System Setup.

As for data collection, two applications were used. An application called LabVIEW was used to read data from the analog lock-in device onto the DAQ, which used two channels to record outputs from the lock-in device, the x and y axes. Thus an overall signal strength could be collected by performing the sum of squares of both these measurements. A Vernier LabQuest device was used to perform temperature measurements. Two Vernier temperature probes were connected to the LabQuest device, which was connected to the Vernier application. The

temperature probes were placed in the hot water and in the surrounding environment to track the temperature of the water over time and get a reading for the room temperature.

4. Results and Discussion

Our team conducted many experiment variations before a successful trial occurred. There are many reasons why the experiment was so difficult to conduct successfully. With the system being extremely sensitive to noise, simply changing positions in the room could alter the amount of radiation being passed into the horn and the receiver. This would result in spikes in voltage that were not reflective of an actual temperature decrease. Furthermore, the experiment depended on the blackbody source being placed as close to the horn as possible. However, the optical chopper had to be angled at 45 degrees to create a signal of radiation passing into the horn. This fact meant that the chopper was placed directly in front of the horn and the blackbody source was placed behind the chopper, and angled away from the horn to avoid radiation being reflected directly back into the horn. Achieving the correct setup was challenging to replicate, and an output voltage would change up to 3 volts, depending on how the black body source was orientated.

This experiment aimed to relate the change in voltage measured by the analog lock-in to the shift in temperature seen by our simulated blackbody and measured by the heterodyne machine. Two main experiments were conducted. The first involved only one source of heat placed behind the optical chopper. When the chopper blocked radiation from passing. This experiment used the ambient room temperature as a reference. The second experiment involved a hot and cold water source that would, over time, reach equilibrium, but had a larger initial temperature difference With the system fully set up to collect data hot water was placed in front of the heterodyne machine angled away from the horn to avoid reflection back into the heterodyne machine, but behind the optical chopper. Another cold water source was placed perpendicular to the horn which would be measured when the optical chopper did not allow

radiation to pass through. The chopper was placed at a 45 degree angle to allow for detection of both the warm water source and the cold. From theoretical predictions the output to the oscilloscope should involve rapid changes in voltage as the heterodyne machine would either measure the hot water source or the cold source. As time went on and the water sources reached equilibrium, our team expected that the voltage fluctuation would converge to a set voltage for the room temperature. However, the signal produced from hot and cold water would initially be a substantial voltage when using the lock-in amplifier and was not observed from the detector observed on the oscilloscope. As the water sources reached equilibrium, the voltage would decrease to "zero" as the sources would produce no variation in the detected radiation when each object was at the same temperature. However, when attempting to conduct this version of the experiment, the output voltage remained constant for most of the time. This could be for a few reasons; the lock-in amplifier was not behaving as expected, the water sources were reflecting radiation into the horn by bouncing off each other, and thus only one signal was seen the entire time, or the system was still too sensitive to noise. The output data mainly was noise with little to do with the actual change in temperature.

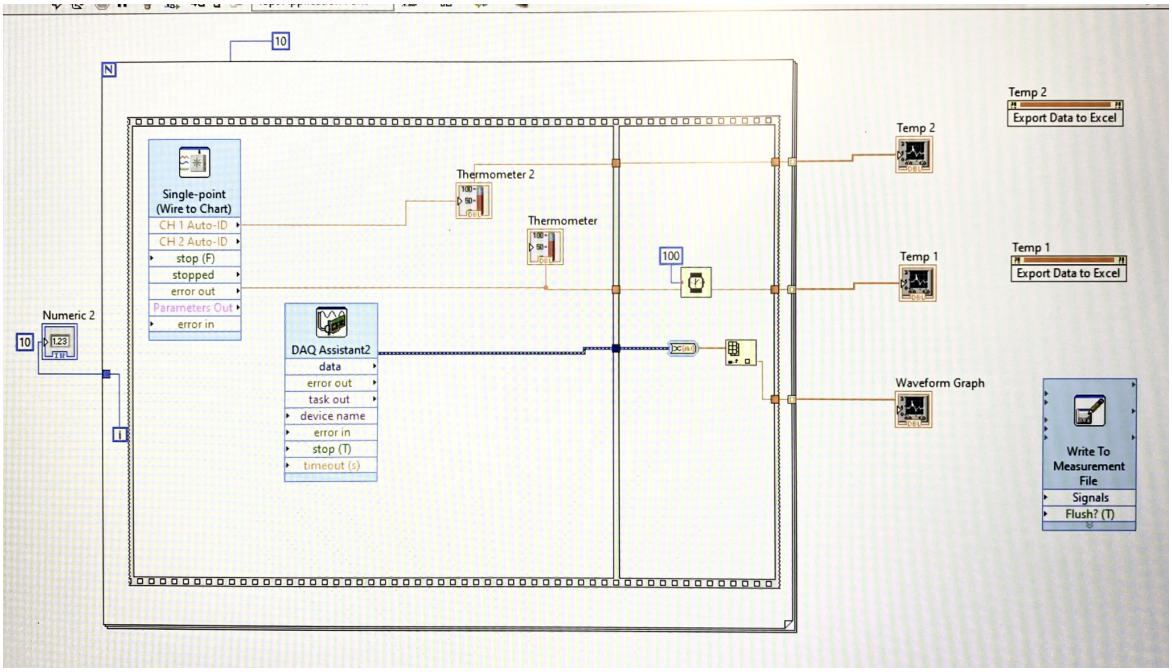

Figure 26. LabVIEW Block Code used to gather data.

Another issue present in the experiment was the process of collecting the data itself. Initially, all data was intended to be collected through LabVIEW (Fig. 26). A loop was intended to interact once every 10 seconds to collect data from the DAQ and the vernier temperature probes. However, the temperature probes would disconnect from the system after an unplanned time, while the DAQ had to run for the remaining portion of the experiment. This casualty resulted in a loss of usable data, impacting the reliability of the results. In order to counteract this issue, it was decided that the DAQ would run in LabVIEW by itself, and the temperature probes would collect data through Vernier Labquest. With the proper experiment set-up finally achieved, a trial was conducted over one hour with a singular black body source. The results are shown in Figure 27.

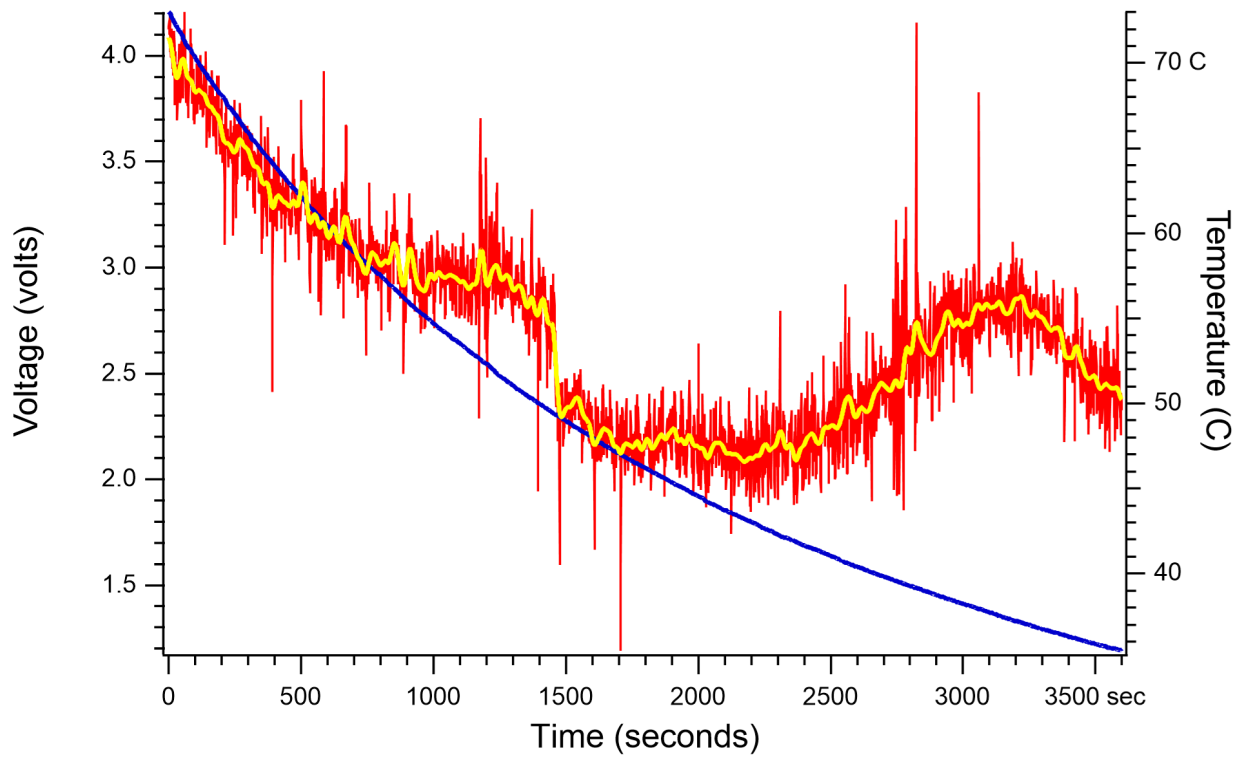

Figure 27. Change in Voltage (thermal power received) and Temperature of the hot water versus Time Graph.

In the figure above, the temperature is represented by the blue line. As measured by the DAQ at a rate of one measurement per second, the voltage can is shown in red, which was smoothed over 120 seconds to produce the yellow line. A few necessary characteristics of this experiment are important to report. First, the decrease in temperature was not linear throughout the entire trial. It appears to be exponential which is predicted by Newton's Law of cooling. From the beginning of the experiment, until about 1000 s, the detected power followed this trend, indicating that the experiment was behaving as expected! However, there is an abrupt increase in voltage after 1000 seconds and again around 2000 seconds. This spike could be from moving around the laboratory and causing increased reflectivities. We hypothesize that moving around the room would result in such drastic change potentially due to reflections of the power leaked

out of the heterodyne receiver. Moving around the room would easily create more interference patterns that affect how the heterodyne receiver gathers input radiation. Likewise, the system's setup may have been too sensitive to accurately record the voltage below a particular temperature. All connections to the amplifiers and power supplies were susceptible to affecting the system when moved.

Regardless of the struggles presented in the data collection of the experiment, the first 1000 seconds did provide valuable data. Figure 28 represents the first 1000 seconds of the trial seen in Figure 27. In this case, the voltage was plotted as a function of temperature, resulting in a strong correlation. In this trial of the experiment, a decrease in 1 degree celsius was correlated to a decrease in about 60.4 millivolts, with an uncertainty of 0.4 millivolts. So the sensitivity of our system was 60.4 mV/^{o}C. The residuals are plotted above the graph, and while slightly skewed, this trial represents a successful proof of concept for the setup. Data for the successful experiment can be found in Appendix B.

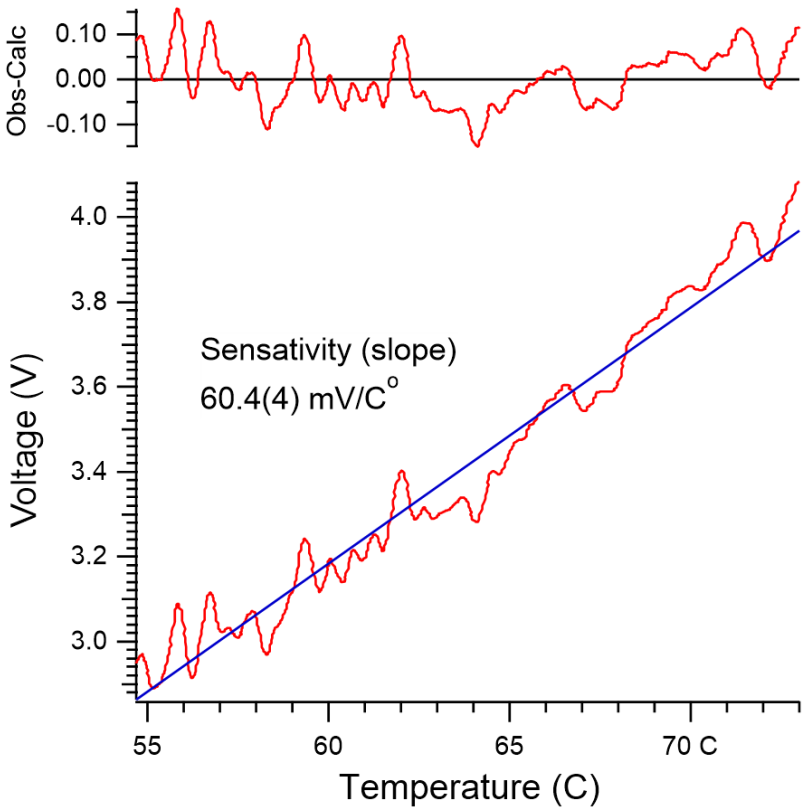

Figure 28. Graph of the First 1000 seconds (s) with Residuals.

5. Recommendations

While our experiment worked as a proof of concept, recommendations could be made to improve the process.

- Firstly, we recommend a more controlled environment for experimentation. With a very touchy system and highly responsive to noise, limiting non-experimental factors on the heterodyne receiver is crucial.
- We also recommend working to replicate data more consistently. While we always placed objects as close as possible concerning the optical chopper, some set-ups would result in unexpected spikes in voltage that did not correlate to temperature differences.
- We recommend experimenting with different materials to simulate a black body. While the mason jar with an open-top models a black body, better materials exist.
- Lastly, we recommend becoming more familiar with the analog lock-in device. We did not collect data on how changing the time constant would affect the change in temperature measured by the heterodyne machine.

Recommendation 1: Controlling Unnecessary Noise

Noise control was crucial in this experiment. Even before the experimentation was conducted, it was easy to be fooled by a false signal when waving a warm object in front of the receiver. The noise present from the amplifier, detector and receiver contributed to the need to bring in the analog lock-in device. While the lock-in amplifier helped to differentiate between the signal being produced from the optical chopper and the system's overall noise, there were still many factors that made controlling the experiment difficult. One of the factors that could be improved upon was the SMA cables being used. The longer the cable, the less accurate and

reliable the signal output is, as the cables do not perfectly trap all of the signals inside. Simply bumping a cable would alter the result to the oscilloscope or lock-in amplifier. Ensuring that the cables used take the shortest path and avoid bends as much as possible would provide more accurate data.

Changing the power to see how the system reacts would be a helpful experiment in later tests. Another problem with the room itself was that the laboratory was not free of people moving around the room. We noticed that when conducting the experiment, if someone's positioning in the room changed, specifically when close to the setup itself, the voltage would spike up on the oscilloscope. We believe this is because the local oscillator 'leaked' out of the system and could be reflected back into the horn as a 'false' signal. One way to avoid this would be to remove people from the room until the investigation is over. While this may be difficult as it is substantial to monitor the experiment, we believe this would help make a more controlled environment.

Another way to control the noise that we attempted but was unsuccessful in our trials is using a different detector to increase the detected bandwidth, B. The detector seen in Figure 16 was passive, which ideally would result in less noise in the system, but was not successful in detecting power. Experimenting with different amplifiers and detectors could improve the overall quality of output into the analog lock-in device. Regardless, attempting to find an amplifier and detector that is the best fit for the output of the heterodyne receiver that has a 20 GHz bandwidth would help improve the signal output and result in more accurate data.

Finding a way to control the noise within our bounds is crucial to the success of this experiment. The ALMA satellite is finely tuned to avoid issues within human control. Still, the reality of the situation is that these measurements are all extremely noisy. It is up to the person

interpreting the data to realize what noise is from human error and what noise cannot be controlled. The light taken from deep within the universe is subject to all types of factors that would result in ‘noise’, such as passing through space dust, being reflected off other objects in space, or simply the fact that the light is traveling over massive distances to reach our observatories. It is not reasonable to expect the ALMA telescopes to extract completely noise-free data, and even the experiment we conducted would require serious effort to get the results to be more accurate and noise-free. Understanding that some degree of noise will always be present is understandable, but we recommend finding a way to eliminate unnecessary interference patterns that cause the data to behave unexpectedly.

Recommendation 2: Consistent Data Replication

The recommendation to replicate data more consistently certainly ties into finding ways to alleviate excessive noise. We ran many trials of this experiment, ranging from 10 minutes to an hour, but did not get the results we intended for. This stems from many factors, ranging from the experiment's environment to the position of equipment used in the experiment. In the early trials of our experiment, we positioned the optical chopper and the black body source further back from the receiver, around 15 centimeters away from the black body source and the chopper around 5 centimeters from the horn. Due to the aperture of the horn, and the beam getting wider as the distance was increased, this resulted in the system picking up on other signals and not the black body itself. To remedy this issue, the optical chopper was placed directly in front of the horn, as close as possible with consideration to the heterodyne receiver itself. The optical chopper was angled at approximately 45 degrees in relation to the horn however ensuring the angle was actually 45 degrees was difficult with our setup. The workstation used as a regular

table without increments for distances. This made it difficult to ensure the chopper was positioned at the proper angle, and more importantly, the black body source could be orientated differently. In the setup for a trial, it was clear that changing the positioning of the blackbody ever so slightly would result in different voltage output. This could be because the black body was not as close to the chopper as it should have been, or more importantly, the angle of the black body and horizontal distance to the horn may have varied. Ideally, the black body would be placed in the same position with the same orientation with respect to the handle every time. This is a reasonably simple way to remedy the issue of non-replicable trials.

Recommendation 3: Experiment with Different Black Bodies

While the black body source of the mason jar represented a hypothetical black body, as radiation and heat via convection escaped from one source at the top and spread to the environment, improvements could be made to make the black body used in the experiment behave more like a theoretical black body. The issue with the mason jar is that the hole at the top was very large, and a smaller hole for radiation and evaporation to escape may have resulted in a better black body source. A key factor for a black body is that it absorbs electromagnetic radiation from all frequencies, regardless of the angle of incidence, and emits black body radiation (Mutlaq, 2021). Our black body was emitting radiation mostly in the infrared region of the electromagnetic spectrum and did not absorb all radiation from the environment without reflecting any back out. In future trials of this experiment, it would be interesting to see the effect of using a different source as a black body. In the lab, certain materials absorb nearly all radiation passed through them. If this were combined with the hot water source, interesting results might occur. Similarly, it would be worthwhile to investigate the phenomena that occur at higher

temperatures. Suppose a piece of carbon was heated to its near melting point. In that case, we infer that the output voltage would be much more reflective of the temperature change, and the system would be able to collect better data over a more extended period of time. With the amplifiers we used, the system may have been unable to read voltage at lower temperatures accurately. Whether the heterodyne receiver would still work when reading extremely high temperatures is unknown, but we theorize it would produce better results than that of boiling water.

Recommendation 4: Experiment with the Lock-in Amplifier More

With the limited time scope of this project, our team felt limited in our ability to use the analog lock-in amplifier. Some recommendations for future trials of this experiment would include changing the sensitivity of the lock-in device to attempt to get more accurate data. The lock-in amplifier would overload when tuned to be too sensitive for measurement. Still, as the temperature cooled, the sensitivity could have been changed as the device would no longer overload. We learned that changing the sensitivity would only alter the output by a proportional amount, and this could have been scaled after the data was collected. However, attempting to do this may have interfered with the heterodyne receiver, as moving around the room would affect the voltage measurement. Another characteristic that would change how the voltage was read is the time constant on the lock-in device. The time constant on the lock-in is used to determine how long the input is measured and then integrated over to return just the signal produced by the optical chopper. By integrating over a longer time period, the results may have been more accurate, but the time constant was set to 1 second for our experiment. If the time constant was set to be larger, the results might have been more accurate. More trials could be conducted at

different sensitivities and time constants if more time were available to see how this would affect the output voltage.

6. Conclusion

Through this project, our team saw many changes from start to finish. Initially, this project's scope was focused on interpreting data from a specific paper published on Betelgeuse that used data from ALMA. Extensive research was conducted on supergiant stars, how ALMA collects data, and various equations used in spectroscopy for astrophysics. This knowledge provided an important base for understanding the effects of black body radiation. However, this focus on ALMA data became extremely theoretical. Due to previous limitations from Covid-19, our team decided that a more hands-on, experimental approach would be the best direction for the project. To accomplish this, the focus was shifted towards how ALMA collects its data instead of the data itself. Doing this meant becoming familiar with how the instrumentation involved with ALMA is used to study black body radiation and finding a way to simulate this in a smaller scale experiment. Along with the decision to go from a more theoretical project to that of experimentation was the desire to use lab equipment present in the WPI physics laboratory. Our advisor recommended we work with a heterodyne receiver that had not been used in the lab before. In a sense, our project was to find a way to use a new piece of equipment and conduct an experiment with it. This detailed research on how a heterodyne receiver operates and what other devices are needed to make it function.

With our team's limited information on the heterodyne receiver, an experiment started to take shape. In the early stages of the experiment, the heterodyne receiver was connected to the radio frequency signal generator for input, and output from the receiver to a detector that was connected to the oscilloscope for voltage output. The detector was connected to a power source and charged with five volts and ground. We had already begun to use five new pieces of lab equipment and understand how they operate. Once it was discovered that the output of the

heterodyne receiver was too weak to be seen on the oscilloscope, an amplifier was introduced to the experiment. To make use of the radio frequency signal generator, the amplifier was tested at varying frequencies and amplitudes to ensure that the detector and amplifier were working properly. Initial trials of the experiment provided hope that the setup was working properly, as placing a hot energy source in front of the receiver would change the signal to the oscilloscope. However, when data was collected, the change in voltage did not model our theoretical predictions. The issue with the experiment was that the components used to boost the signal out of the heterodyne receiver created too much noise. In an attempt to handle the noise in the system, an optical chopper and an analog lock-in device were introduced to the experiment. By creating a frequency of radiation passing through the chopper or not, the analog lock-in amplifier could integrate the signal over time and return just the signal without noise from the other components. This was a major stepping stone in the project, as useful data could finally be collected. However, through trial and error, we learned that the positioning of the optical chopper and our hypothetical black body source of hot water in a mason needed to be properly orientated to avoid direct radiation being reflected into the heterodyne receiver.

Furthermore, we learned that the horn of the receiver would take input from the environment as the beam spreads as the distance to the object increases. With this in mind, a successful trial of the experiment was conducted, with the optical chopper positioned directly in front of the horn and the black body source immediately behind the optical chopper. The experiment ran for one hour and provided useful data from the first 1000 seconds before other factors skewed some of the data. With the valuable data, we were able to provide a proof of concept of a working temperature sensor that resulted in a measured sensitivity of the system of about 60 millivolts per degree celsius. Further experiments were conducted using two

temperature sources or different detectors but proved unsuccessful in initial trials. As the timeline to conclude the project is rapidly approaching, our successful trial was deemed sufficient progress. Our team investigated a piece of equipment previously unused by the physics department and was able to provide a proof of concept for how a heterodyne receiver functions.

We gained plenty of hands-on experience with different lab equipment that we were mainly looking for in this process. Likewise, we are now more familiar with how ALMA collects its data. This is extremely useful as astrophysics is a promising field for the future, and this insight is important to have for when future discoveries occur. With this in mind, we consider our MQP project a success. We are happy and proud of our accomplishments with many ups and downs, which is typical for any research project and experiment.

Appendix A: Data Sheet for Power Detector Calibration Test.

dB	V at 8Ghz	V at 6Ghz	V at 5Ghz	V at 2 Ghz	V at 1 Ghz	V at 10 Mhz
-60				2.06	2.07	
-59				2.04	2.06	
-58				2.02	2.04	
-57				2	2.03	
-56				1.98	2.01	
-55			2.07	1.96	1.99	1.97
-54			2.05	1.94	1.97	1.95
-53			2.04	1.92	1.95	1.93
-52			2.02	1.89	1.92	1.91
-51			2	1.87	1.9	1.89
-50	2.09	2.01	1.97	1.84	1.88	1.87
-49	2.08	1.99	1.95	1.82	1.85	1.85
-48	2.07	1.97	1.92	1.79	1.83	1.82
-47	2.06	1.94	1.9	1.77	1.8	1.8
-46	2.05	1.92	1.87	1.74	1.78	1.78
-45	2.03	1.9	1.85	1.72	1.76	1.76
-44	2.01	1.87	1.82	1.69	1.73	1.73
-43	2	1.85	1.8	1.67	1.71	1.71
-42	1.98	1.82	1.77	1.64	1.68	1.69
-41	1.96	1.8	1.75	1.62	1.65	1.66
-40	1.94	1.77	1.72	1.59	1.63	1.64
-39	1.92	1.75	1.7	1.57	1.6	1.61
-38	1.9	1.73	1.67	1.54	1.58	1.59
-37	1.88	1.7	1.65	1.52	1.55	1.57
-36	1.86	1.67	1.62	1.49	1.53	1.54
-35	1.83	1.65	1.6	1.47	1.51	1.52
-34	1.81	1.62	1.57	1.45	1.48	1.49
-33	1.79	1.59	1.55	1.42	1.46	1.47
-32	1.76	1.57	1.52	1.4	1.43	1.45
-31	1.74	1.55	1.5	1.37	1.41	1.42
-30	1.72	1.52	1.47	1.35	1.38	1.4
-29	1.7	1.5	1.45	1.32	1.36	1.37
-28	1.67	1.47	1.42	1.3	1.33	1.35
-27	1.65	1.45	1.4	1.27	1.31	1.32
-26	1.63	1.42	1.37	1.25	1.28	1.3

-25	1.61	1.4	1.35	1.22	1.26	1.273
-24	1.58	1.37	1.32	1.197	1.23	1.247
-23	1.56	1.35	1.3	1.171	1.21	1.222
-22	1.54	1.32	1.27	1.146	1.18	1.197
-21	1.52	1.3	1.25	1.122	1.15	1.172
-20	1.49	1.275	1.22	1.097	1.13	1.147
-19	1.47	1.25	1.2	1.072	1.11	1.122
-18	1.45	1.225	1.17	1.048	1.083	1.096
-17	1.42	1.2	1.15	1.022	1.057	1.071
-16	1.4	1.176	1.12	0.997	1.031	1.045
-15	1.38	1.151	1.1	0.973	1.005	1.02
-14	1.36	1.128	1.07	0.948	0.981	0.994
-13	1.33	1.104	1.05	0.922	0.956	0.969
-12	1.31	1.078	1.02	0.897	0.931	0.934
-11	1.28	1.052	0.999	0.871	0.906	0.918
-10	1.26	1.026	0.974	0.845	0.88	0.892
-9	1.23	1.001	0.958	0.817	0.854	0.865
-8	1.21	0.977	0.923	0.791	0.827	0.838
-7	1.18	0.953	0.899	0.763	0.8	0.811
-6	1.16	0.929	0.875	0.737	0.773	0.785
-5	1.13	0.905	0.849	0.711	0.747	0.758
-4	1.1	0.88	0.822			0.733
-3	1.08	0.854	0.796			0.708
-2	1.06	0.827	0.769			0.684
-1	1.03	0.8	0.742			0.662
0	1	0.774	0.716			0.641
1	0.975	0.749	0.691			
2	0.947	0.726	0.669			
3	0.92	0.702	0.647			
4	0.894	0.68	0.625			
5	0.87	0.66	0.605			

Appendix B: First 3 minutes of data from the successful run of the experiment

The full data sheet can be accessed through the following link:

Successful Trial of Experiment (1 hour) (1).xlsx

Time (s)	Voltage y-out (V)	Voltage x-out (V)	Sum of Squares (V)	Temperature of Hot Water (C)	Temperature of Room (C)
0	0.278285	4.115972	4.125368838	73.00517422	21.44005264
1	0.120686	4.137029	4.13878896	73.00517422	21.46490645
2	0.459574	4.141306	4.166728171	72.95217934	21.44005264
3	0.221365	4.094585	4.100564447	72.95217934	21.44005264
4	0.407918	4.137358	4.157418468	72.90236991	21.44005264
5	0.391138	4.17717	4.195442544	72.90236991	21.44005264
6	0.011452	4.01891	4.018926316	72.90236991	21.44005264
7	0.229261	4.118933	4.125308433	72.90236991	21.44005264
8	0.833996	3.905068	3.993132281	72.84951952	21.44005264
9	0.690873	4.001801	4.060999476	72.79984565	21.44005264
10	0.192412	4.064973	4.06952428	72.79984565	21.44005264
11	0.239132	4.12321	4.130138595	72.69759967	21.44005264
12	0.317767	3.984033	3.996685478	72.64503553	21.44005264
13	-0.159637	3.959686	3.962902622	72.64503553	21.44005264
14	-0.317237	3.924151	3.936953186	72.64503553	21.44005264
15	-0.361654	3.966924	3.983375408	72.54320789	21.44005264
16	-0.071132	3.97515	3.975786373	72.59563023	21.44005264
17	-0.069157	4.003775	4.004372228	72.49393563	21.44005264
18	0.0789	3.904081	3.904878188	72.49393563	21.46490645
19	0.134175	3.958041	3.960314569	72.4416542	21.44005264
20	0.173328	4.10314	4.106799296	72.4416542	21.46490645
21	0.695151	4.057735	4.11684931	72.4416542	21.44005264
22	0.865253	3.949815	4.043476387	72.39251415	21.46490645
23	0.431278	3.746808	3.771547547	72.34037275	21.46490645
24	0.15622	3.765233	3.7684724	72.34037275	21.44005264
25	-0.049087	3.846831	3.847144171	72.2913641	21.46490645
26	-0.226757	4.014962	4.021360292	72.23936188	21.46490645
27	-0.135619	3.864269	3.866648086	72.23936188	21.46490645
28	-0.377776	3.93139	3.94949896	72.19048381	21.46490645
29	-0.060274	3.790239	3.790718221	72.23936188	21.48829598
30	0.225642	3.816561	3.823225363	72.19048381	21.46490645
31	0.036128	3.760627	3.760800535	72.13861991	21.46490645
32	0.381268	3.674094	3.693823495	72.08987162	21.46490645
33	0.355604	3.764246	3.781005442	72.08987162	21.46490645
34	0.485566	3.930403	3.960283081	72.04118596	21.46490645
35	0.225971	3.775104	3.781861064	72.04118596	21.46490645
36	-0.050732	3.792871	3.793210271	72.04118596	21.46490645
37	-0.021121	3.862295	3.86235275	71.98952587	21.48829598
38	0.214456	3.92119	3.927050088	71.88944495	21.46490645
39	0.336192	4.043916	4.057866641	71.88944495	21.48829598
40	0.065411	3.972847	3.973385444	71.88944495	21.46490645
41	-0.097782	4.055102	4.056280753	71.8410157	21.46490645
42	0.453981	3.96824	3.994124115	71.8410157	21.46490645
43	0.987648	3.773459	3.900569368	71.8410157	21.46490645

44	0.348037	3.762601	3.778663261	71.8410157	21.46490645
45	0.48425	3.772472	3.803425174	71.78962722	21.46490645
46	0.3737	3.947512	3.965161117	71.78962722	21.46490645
47	0.173658	4.032729	4.036466312	71.69007109	21.46490645
48	0.330599	4.054115	4.067572265	71.74132501	21.48829598
49	0.164774	4.038322	4.041682205	71.69007109	21.46490645
50	0.181225	4.017265	4.021350592	71.69007109	21.48829598
51	0.133846	4.110049	4.112227807	71.64189514	21.46490645
52	0.022638	4.101166	4.101228479	71.64189514	21.48829598
53	-0.174114	3.793858	3.797851262	71.59077497	21.46490645
54	-0.010592	4.054444	4.054457835	71.44381156	21.46490645
55	-0.060274	4.053786	4.054234069	71.39295645	21.46490645
56	-0.155031	3.954092	3.95713004	71.39295645	21.48829598
57	0.348695	3.9077	3.923226669	71.39295645	21.48829598
58	0.385874	4.107088	4.125175219	71.34515471	21.48829598
59	0.062779	4.107088	4.107567777	71.29443093	21.46490645
60	0.21643	4.201847	4.207417279	71.29443093	21.46490645
61	0.71193	3.986008	4.049086823	71.24675243	21.48829598
62	0.897826	3.974163	4.074317498	71.24675243	21.46490645
63	1.241321	3.854398	4.049353253	71.24675243	21.48829598
64	0.981067	3.822812	3.946692799	71.1486032	21.48829598
65	0.364817	3.760627	3.778280942	71.1486032	21.48829598
66	-0.140225	3.862295	3.864839676	71.1486032	21.51314492
67	0.242093	3.771485	3.779247032	71.09813972	21.48829598
68	0.06245	3.838276	3.838784007	71.05070548	21.48829598
69	-0.052049	3.871837	3.872186831	71.05070548	21.48829598
70	-0.146147	3.936325	3.939037122	71.05070548	21.48829598
71	-0.052707	3.763917	3.764286016	71.00037099	21.48829598
72	0.415485	3.832025	3.854483543	70.95305778	21.46490645
73	0.221365	3.781026	3.787500505	70.9028515	21.48829598
74	0.774773	3.623425	3.705331555	70.9028515	21.48829598
75	1.18111	3.586245	3.7757349	70.9028515	21.51314492
76	0.58131	3.831696	3.875540679	70.9028515	21.48829598
77	0.392125	3.893223	3.912920564	70.8556586	21.48829598
78	0.307897	3.852424	3.864708429	70.80557977	21.48829598
79	-0.178391	3.922835	3.926889072	70.8556586	21.48829598
80	0.11575	3.888617	3.890339347	70.8556586	21.51314492
81	0.364817	3.861966	3.879158778	70.8556586	21.51314492
82	0.387519	3.86394	3.883323744	70.75850647	21.51314492
83	0.081862	4.127816	4.128627655	70.71149089	21.48829598
84	-0.14878	4.056089	4.058816757	70.75850647	21.51314492
85	-0.174772	4.049509	4.053278721	70.71149089	21.51314492
86	0.122989	3.955737	3.957648482	70.71149089	21.51314492
87	0.369094	3.90112	3.918541519	70.66159992	21.51314492
88	0.378964	3.812942	3.831728123	70.66159992	21.48829598

89	0.279272	3.997852	4.007594473	70.61470288	21.48829598
90	0.022638	3.772801	3.772868917	70.56493748	21.48829598
91	0.185831	3.782343	3.786905297	70.56493748	21.48829598
92	0.700415	3.822483	3.886123706	70.5181583	21.51314492
93	0.459574	3.911319	3.93822607	70.5181583	21.48829598
94	-0.143844	3.815903	3.818613204	70.5181583	21.51314492
95	-0.241892	3.687584	3.695509098	70.46851773	21.51314492
96	0.000923	3.738583	3.738583114	70.46851773	21.51314492
97	-0.024082	3.823141	3.823216846	70.37233923	21.48829598
98	-0.063235	3.677055	3.677598692	70.42185569	21.51314492
99	0.303948	3.811626	3.823725559	70.37233923	21.48829598
100	0.148323	3.807019	3.809907266	70.32579365	21.51314492
101	0.119699	3.733318	3.735236424	70.27640056	21.48829598
102	0.406602	3.70239	3.724649903	70.27640056	21.51314492
103	0.039089	3.774446	3.774648402	70.27640056	21.48829598
104	0.021651	3.785304	3.785365919	70.22997076	21.51314492
105	0.865253	3.660604	3.7614737	70.22997076	21.51314492
106	0.827745	3.876772	3.964154755	70.13438561	21.48829598
107	0.332244	3.91461	3.928683943	70.0852371	21.51314492
108	-0.104691	3.949815	3.951202189	70.0852371	21.53652989
109	0.000265	3.727725	3.727725009	70.0852371	21.51314492
110	0.27006	3.861966	3.871396878	70.0852371	21.48829598
111	0.088771	3.846502	3.847526209	70.0852371	21.51314492
112	0.407918	3.880062	3.901445658	70.03903681	21.51314492
113	0.450361	3.936983	3.962658221	70.03903681	21.53652989
114	0.369423	3.861637	3.879267157	69.94392299	21.51314492
115	0.160497	3.784646	3.788047602	69.94392299	21.51314492
116	0.013097	3.87743	3.877452119	69.94392299	21.51314492
117	-0.036914	3.803729	3.803908115	69.89501622	21.53652989
118	0.005201	3.768524	3.768527589	69.89501622	21.51314492
119	-0.013553	3.781355	3.781379288	69.84904278	21.51314492
120	-0.204713	3.998839	4.004075519	69.84904278	21.53652989
121	-0.059616	3.745821	3.746295374	69.84904278	21.53652989
122	0.460232	3.74944	3.777580417	69.80025583	21.48829598
123	0.205572	3.915597	3.920989634	69.75439483	21.48829598
124	-0.118181	3.893552	3.895345161	69.75439483	21.53652989
125	-0.312301	3.768853	3.781770068	69.75439483	21.53652989
126	0.080875	3.863611	3.864457365	69.70572699	21.53652989
127	0.394099	3.763588	3.784165516	69.70572699	21.53652989
128	0.936321	3.617173	3.736393653	69.61142837	21.51314492
129	1.226844	3.502016	3.710695658	69.61142837	21.53652989
130	0.929082	3.613883	3.731399697	69.61142837	21.53652989
131	0.298355	3.708971	3.720951704	69.5657903	21.53652989
132	0.330599	3.755363	3.769886863	69.5657903	21.53652989
133	0.508268	3.883352	3.91647279	69.51735864	21.51314492
134	0.361527	3.87414	3.890971924	69.51735864	21.53652989

135	-0.023753	3.953763	3.95383435	69.47183108	21.53652989
136	0.016387	3.87414	3.874174657	69.47183108	21.51314492
137	-0.01487	3.911977	3.912005261	69.37809879	21.53652989
138	-0.335004	3.736608	3.751595264	69.37809879	21.53652989
139	-0.371853	3.784975	3.803197392	69.37809879	21.51314492
140	-0.092189	4.019897	4.020953954	69.37809879	21.53652989
141	0.241106	3.986337	3.993621762	69.33273413	21.53652989
142	-0.151741	3.788923	3.791960289	69.33273413	21.51314492
143	0.451019	3.728383	3.755563597	69.33273413	21.53652989
144	1.139325	3.377317	3.564313619	69.33273413	21.53652989
145	0.649088	3.654682	3.711874965	69.33273413	21.53652989
146	0.072649	3.716867	3.717576922	69.19130983	21.53652989
147	-0.230705	3.806361	3.81334615	69.23933641	21.53652989
148	0.416802	3.764575	3.787578229	69.19130983	21.53652989
149	0.507281	3.741215	3.775450131	69.14616241	21.53652989
150	0.05883	3.643824	3.644298878	69.14616241	21.51314492
151	-0.243537	3.640534	3.648670727	69.09825058	21.53652989
152	-0.27249	3.653695	3.663841966	69.14616241	21.56137403
153	-0.258013	3.839921	3.848579477	69.14616241	21.56137403
154	-0.111601	3.858018	3.859631805	69.09825058	21.51314492
155	0.108841	3.610593	3.612233129	69.09825058	21.56137403
156	0.468128	3.686926	3.716526221	69.00541312	21.53652989
157	0.249332	3.736608	3.744917328	69.00541312	21.56137403
158	0.035799	3.775762	3.775931706	69.00541312	21.53652989
159	0.123318	3.785633	3.787641026	69.00541312	21.53652989
160	0.222681	3.824457	3.830934373	69.00541312	21.53652989
161	0.275653	3.70568	3.715918304	68.96048047	21.56137403
162	0.443452	3.800768	3.826550283	68.96048047	21.53652989
163	0.766218	3.78662	3.863363955	68.91279619	21.56137403
164	0.570124	3.889933	3.931490827	68.86797002	21.53652989
165	0.191424	3.76293	3.767795819	68.82039853	21.56137403
166	-0.063564	3.721473	3.722015808	68.82039853	21.56137403
167	0.076268	3.881707	3.882456187	68.77567823	21.53652989
168	0.243738	3.69581	3.703838518	68.77567823	21.56137403
169	-0.16885	3.700745	3.704594968	68.77567823	21.56137403
170	-0.139238	3.616186	3.618865624	68.72821892	21.56137403
171	0.312174	3.724106	3.737167123	68.68360389	21.53652989
172	0.280259	3.630992	3.641791868	68.68360389	21.56137403
173	0.290459	3.71588	3.727214859	68.68360389	21.53652989
174	0.540512	3.743847	3.782663556	68.63625611	21.56137403
175	0.150297	3.806361	3.809327139	68.59174575	21.56137403
176	-0.360667	3.592826	3.610883459	68.59174575	21.56137403
177	-0.4801	3.642837	3.674337684	68.59174575	21.56137403
178	-0.05139	3.670804	3.671163704	68.54450888	21.56137403
179	0.811623	3.437857	3.532363606	68.54450888	21.56137403
180	0.9735	3.476023	3.609769819	68.50010262	21.56137403

6. References

1. ALMA — Science Website. (n.d.). Retrieved April 28, 2022, from ALMA — Science Website
2. APITech. (n.d.). RF Amplifiers. Retrieved April 28, 2022, from RF Amplifiers
3. Betelgeuse | Size, Dimming, Color, Meaning, & Facts | Britannica. (n.d.). Retrieved April 28, 2022, from Betelgeuse | Size, Dimming, Color, Meaning, & Facts | Britannica
4. Blackbody Radiation. (2022, February 20). https://phys.libretexts.org/@go/page/4520
5. Briggs, A. (2020, January 7). Betelgeuse: What's up? EarthSky. Retrieved February 1, 2022, from Betelgeuse: What's up? | Space | EarthSky
6. Briggs, A. (2021, June 6). What is a variable star? EarthSky. Retrieved February 1, 2022, from What is a variable star?
7. Britannica, T. Editors of Encyclopedia (2020, April 8). Planck's radiation law. Encyclopedia Britannica. Planck's radiation law | Definition, Formula, & Facts | Britannica
8. Britannica, T. Editors of Encyclopedia (2021, November 30). Planck's constant. Encyclopedia Britannica. Planck's constant | Definition, Units, Symbol, & Facts | Britannica
9. Buitenen, J. Van, Lin, Chao, Schmidt, John D., Bickerman, E.J. Ziadeh, Nicola Abdo, Wiesenberg, E.J. Proskouriakoff, Tatiana and Ronan, . Colin Alistair (2021, October 21). calendar. Encyclopedia Britannica. Retrieved January 20, 2022, from calendar | chronology | Britannica
10. Crockett, C. (2019). What is the electromagnetic spectrum? | Space | EarthSky. What is the electromagnetic spectrum? | Space | EarthSky
11. Ehrenfreund, P., & Cami, J. (2010). Cosmic Carbon Chemistry: From the Interstellar Medium to the Early Earth. Cold Spring Harbor Perspectives in Biology, 2(12), a002097. https://doi.org/10.1101/cshperspect.a002097
12. Factsheet | ALMA. (n.d.). Retrieved April 29, 2022, from Factsheet | ALMA
13. Gohd, C. (2021, January 8). Astronomers reevaluate the age of the universe. Space.com. Retrieved January 20, 2022, from Astronomers reevaluate the age of the universe | Space
14. Hajian, A. (2011). Shedding a New Light on the Universe - Frequency, Wavelength, Energy Activity. Shedding a New Light on the Universe - Frequency, Wavelength, Energy Activity
15. Hall, J. C. (2018, May 23). ." The gale encyclopedia of science. . encyclopedia.com. 24 Jan. 2022. Encyclopedia.com. Retrieved January 25, 2022, from Hertzsprung-russell Diagram | Encyclopedia.com
16. Herbst, E. (1995). Chemistry in the interstellar medium. Annual Reviews. Retrieved January 20, 2022, from Chemistry in the Interstellar Medium
17. Hertzsprung-Russell Diagram: Cosmos. Hertzsprung-Russell Diagram | COSMOS. (n.d.). Retrieved January 25, 2022, from Hertzsprung-Russell Diagram | COSMOS
18. Howell, E. (2017, May 18). How many stars are in the universe? Space.com. Retrieved January 20, 2022, from How many stars are in the universe? | Space

19. Iida, T., & Wakana, H. (2003). Communications Satellite Systems. In R. A. Meyers (Ed.), Encyclopedia of Physical Science and Technology (Third Edition) (pp. 375–408). Academic Press. https://doi.org/10.1016/B0-12-227410-5/00882-6
20. Joardar, S., Bhattacharyya, S., Bhattacharya, A., & Datta, C. (2010). Radio Astronomy and Super-Synthesis: a Survey. Progress In Electromagnetics Research B, 22, 73–102. https://doi.org/10.2528/PIERB10032105
21. Levesque, E. M., Massey, P., Olsen, K. a. G., Plez, B., Josselin, E., Maeder, A., & Meynet, G. (2005). The Effective Temperature Scale of Galactic Red Supergiants: Cool, but Not as Cool as We Thought. *The Astrophysical Journal*, *628*(2), 973. The Effective Temperature Scale of Galactic Red Supergiants: Cool, but Not as Cool as We Thought - IOPscience
22. Lock-in Amplifier. (n.d.). PhysicsOpenLab. Retrieved April 28, 2022, from https://physicsopenlab.org/2019/08/20/lock-in-amplifier/
23. Morata, O., & Huang, T. (2017). ALMA's long look. Nature Astronomy, 1(6), 0156. ALMA's long look | Nature Astronomy
24. Moskowitz, C. (2013, March 8). 8 Cool Facts About the ALMA Telescope. Space.Com. 8 Cool Facts About the ALMA Telescope | Space
25. Mutlaq, J. (n.d.). Blackbody Radiation. Retrieved April 28, 2022, from Blackbody Radiation
26. NASA. (n.d.). Background: Life cycles of stars. NASA. Retrieved January 20, 2022, from Background: Life Cycles of Stars
27. Planck's constant | Definition, Units, Symbol, & Facts | Britannica. (n.d.). Retrieved April 12, 2022, from https://www.britannica.com/science/Plancks-constant
28. Receivers | ALMA. (n.d.). Retrieved April 28, 2022, from https://www.almaobservatory.org/en/about-alma/how-alma-works/technologies/receivers
29. Spotts, I., Brodie, C. H., Gadsden, S. A., Al-Shabi, M., & Collier, C. M. (2021). A comparison of nonlinear filtering methods for blackbody radiation applications in photonics. Optics and Photonics for Information Processing XV, 11841, 139–148. https://doi.org/10.1117/12.2594674
30. Stars and Nebulas. HubbleSite.org. (n.d.). Retrieved January 20, 2022, from STARS AND NEBULAS
31. Stars. (n.d.). National Schools' Observatory. Retrieved January 20, 2022, from Stars | National Schools' Observatory
32. Supergiant stars: Facts, information, history & definition. The Nine Planets. (2021, January 4). Retrieved February 1, 2022, from Supergiant Stars | Facts, Information, History & Definition
33. Terahertz Properties. (n.d.). TOPTICA Photonics AG. Retrieved April 28, 2022, from Terahertz Properties | TOPTICA Photonics AG
34. Ulaby, F., & Long, D. (2015). Microwave Radar and Radiometric Remote Sensing. Artech House. http://ebookcentral.proquest.com/lib/wpi/detail.action?docID=4537961
35. Wallrabe, U., & Mohr, J. (2008). 1.11.3.2.4 Heterodyne receiver. In *Comprehensive microsystems* (Vol. 1). essay, Elsevier. From, https://www.sciencedirect.com/topics/engineering/heterodyne-receiver

36. Wolstencroft, R. D., & Burton, W. B. (2012). Millimeter and Submillimetre Astronomy: Lectures Presented at a Summer School Held in Stirling, Scotland, June 21–27, 1987. Springer Science & Business Media.
37. Zel'dovich, Y. B. (1975). Interaction of free electrons with electromagnetic radiation. Soviet Physics Uspekhi, 18(2), 79. https://doi.org/10.1070/PU1975v018n02ABEH001947
38. Zhang, Y., Li, Q., & Zhou, H. (2016). Theoretical Foundation and Basic Properties of Thermal Radiation. In Theory and Calculation of Heat Transfer in Furnaces (pp. 1–43). Elsevier. https://doi.org/10.1016/B978-0-12-800966-6.00001-6